Theory of ITG turbulent saturation in stellarators: identifying mechanisms to reduce turbulent transport

C. C. Hegna, P. W. Terry and B. J. Faber
Departments of Engineering Physics and Physics,
University of Wisconsin-Madison, Madison, WI 53706

A three-field fluid model that allows for general three-dimensional equilibrium geometry is developed to describe ion temperature gradient turbulent saturation processes in stellarators. The theory relies on the paradigm of nonlinear transfer of energy from unstable to damped modes at comparable wavelength as the dominant saturation mechanism. The unstable-to-damped mode interaction is enabled by a third mode that for dominant energy transfer channels primarily serves as a regulator of the nonlinear energy transfer rate. The identity of the third wave in the interaction defines different scenarios for turbulent saturation with the dominant scenario depending upon the properties of the 3D geometry. The nonlinear energy transfer physics is quantified by the product of a turbulent correlation lifetime and a geometric coupling coefficient. The turbulent correlation time is determined by a three-wave frequency mismatch, which at long wavelength can be calculated from the sum of the linear eigenfrequencies of the three modes. Larger turbulent correlation times denote larger levels of nonlinear energy transfer and hence smaller turbulent transport. The theory provides an analytic prediction for how 3D shaping can be tuned to lower turbulent transport through saturation processes.

Pacs. nos. 52.35.Ra, 52.55.Hc, 52.35.Kt, 52.55.Dy

I. INTRODUCTION

An analytic theory for turbulent saturation of ion temperature gradient (ITG) driven turbulence is developed for general three-dimensional (3D) magnetic configurations. The theory relies on the premise that coupling of linearly unstable eigenmodes to damped eigenmodes of comparable wave number is the dominant saturation process [1–3]. A primary motivation for this work is to distinguish mechanisms associated with magnetic geometry that affect turbulent transport in stellarator experiments. Here, we show that nonlinear energy transfer from unstable to damped modes is enabled by a three-wave interaction, where the third mode depends upon the properties of the 3D shaping. The theory developed in the following identifies an important metric, the product of a turbulent correlation lifetime and a geometric coupling coefficient, that quantifies nonlinear energy transfer. Large values of this metric correspond to small values of ITG-induced turbulent transport. We anticipate that the results of this work can be used to guide optimization schemes to produce stellarator designs with lowered turbulent transport.

In stellarator configurations, plasma performance is largely dictated by the external magnetic field, with 3D shaping allowing considerable design flexibility. As such, optimization procedures have been developed to target specific physics goals in stellarator design [4]. Prominently, notions for optimizing neoclassical transport, a traditional weakness for conventional stellarators, have emerged with the identification of quasi-omnigeneity [5, 6] and quasi-symmetry [7, 8] as promising approaches to stellarator confinement. Neoclassical transport optimization is the defining aspect of the present generation of stellarator designs [9–12].

Having made significant progress in controlling neoclassical transport, the next frontier for confinement optimization in stellarators is turbulent transport. There have been efforts to ask how 3D shaping may be used to reduce microturbulence in plasmas. The bulk of these studies seek to minimize the peak linear growth rate in optimization studies appealing to a mixing length estimate ($\chi \sim \gamma/k_\perp^2$) for transport coefficients [13–16]. However, linear stability does not provide the complete picture for turbulent transport in magnetic confinement devices [17]. In this paper, we work towards developing a theory for turbulent saturation of ITG driven turbulence in stellarators. The motivation is to find mechanisms by which 3D shaping can be used to affect turbulent transport.

Neoclassical optimization of electron heat transport has been successfully demonstrated in the Helically Symmetric Experiment (HSX) [18]. In these electron heated experiments, anomalous transport dominates predictions for neoclassical transport, with trapped electron mode (TEM) turbulence being a likely candidate to explain these observations [19–22]. Microinstabilities are thought to be a weakness of quasi-helically symmetric (QHS) configurations like HSX, as normalized linear growth rates are generally much larger in QHS relative to other stellarator configurations [16, 23]. This shortcoming is largely due to the relatively short connection lengths present in QHS affecting both microinstability and ideal ballooning stability [24]. However, comparisons of nonlinear gyrokinetic simulations of TEM turbulence in HSX [16] and Wendelstein 7-X [25] geometries show that these two configurations have comparable turbulent transport rates in gyro-Bohm units. This suggests that there may be some intrinsic advantage to QHS with regard to turbulent saturation physics. Indeed, HSX confinement scalings are comparable to predictions using stellarator empirical scalings [26] despite their apparent disadvantages with regard to linear microinstabilities. More generally, if underlying principles for affecting turbulent saturation can be identified in 3D configurations, these may be exploited in stellarator optimization schemes.

To describe turbulent saturation, we utilize a model that concentrates on the role of damped eigenmodes [1–3]. In this model, the dominant energy transfer occurs from unstable to stable modes at comparable wavenumber. This mechanism is distinct from other approaches which rely on zonal flow shearing or energy cascades to dissipative scales [27–29]. This work identifies key metrics for turbulent saturation that are purely a property of the nonlinear dynamics. The strength of the nonlinear transfer rate is quantified by nonlinear correlation times derived from the sum of a three-wave frequency mismatch. The three waves of interest are an instability at wavenumber $\mathbf{k}$, a damped mode at mode number $\mathbf{k}'$, and a coupling mode at $\mathbf{k} - \mathbf{k}'$. The identity of the third wave in this interaction defines different scenarios for turbulent saturation. The dominant scenario depends upon the properties of the 3D geometry.

As an application of theory, we quantify these metrics for two classes of quasi-symmetric stellarator configurations: quasi-axisymmetry (QAS) and quasi-helical symmetry (QHS). In QAS configurations, the dominant linear ITG eigenmodes resemble the 'toroidal' ITG modes that dominate tokamak turbulence. In this case, the zonal flow plays an important role, mediating the transfer between the unstable modes and damped eigenmodes [2, 3].

For QHS configurations, the dominant linear ITG mode structure has a more 'slab-like' feature, owing to the short connection length, which leads to larger linear instability growth rates. However, we find that besides zonal flow-mediated nonlinear transfer, there are additional three-wave interactions that also play an important role in the saturation physics. In this additional energy transfer channel, a nearly marginally stable non-zonal eigenmode plays the role of a mediator for nonlinear transfer. This suggests there are additional mechanisms available in QHS configurations that can accessed for lower turbulent transport. As such, there may be an inherent advantage to QHS geometry that could be exploited in future optimization studies.

Zonal flow physics has received considerable attention in the stellarator community in the past decade [30–34]. A

distinguishing feature of zonal flows in 3D configurations is that they can be collisionlessly damped in the presence of particles with a net bounce averaged radial drift. As particles with net radial drift enhance neoclassical transport, this suggests that if zonal flow dynamics are important in establishing turbulent saturation that optimizing for good neoclassical properties can also aid in reducing turbulent transport [32, 35, 36]. Indeed, in the limit of large zonal flow damping, the turbulence level scales with the damping rate [37]. The calculation presented in the following supports this observation.

In the following section, we introduce notation for the magnetic field quantities and identify key geometric coefficients. In section III, the basic three-field model for ITG turbulence using an adiabatic electron approximation is introduced. Building on prior ITG studies where simple geometric models [38, 39] were employed to emphasize the nonlinear phyiscs, we develop a model for ITG turbulent saturation that accommodates general 3D geometry. In Section IV, linear properties of this system are described. In Section V, a nonlinear saturation model is derived relying on the premise that turbulent saturation is controlled by nonlinear transfer from unstable to stable eigenmodes. In this section, possible proxies for stellarator optimization are identified. We summarize this work in Section VI and comment on future avenues for study.

II. MAGNETIC GEOMETRY

In this section, notation for the magnetic geometry is introduced. Important geometric quantities for ITG turbulence in 3D configurations are identified.

The equilibrium magnetic field is written

$$\mathbf{B} = \nabla\psi \times \nabla\theta + \iota\nabla\zeta \times \nabla\psi = \frac{d\psi}{d\rho}\nabla\rho \times \nabla\alpha, \tag{1}$$

where ρ is a "radial" like variable with $\psi = \psi(\rho)$ denoting the toroidal flux surface label, $\psi' = d\psi/d\rho$ and $\alpha = \theta - \iota\zeta$ for straight field-line poloidal angle θ, toroidal angle ζ and rotational transform ι. The curvature vector $[\vec{\kappa} = (\hat{\mathbf{b}}\cdot\nabla)\hat{\mathbf{b}}]$ can be written

$$\vec{\kappa} = \kappa_n\hat{\mathbf{n}} + \kappa_g\hat{\mathbf{b}} \times \hat{\mathbf{n}}, \tag{2}$$

where $\hat{\mathbf{n}} = \nabla\rho/|\nabla\rho|$ and $\mathbf{b} = \mathbf{B}/|B|$, with the normal (geodesic) component of the curvature denoted κ_n (κ_g). The local shear is defined by

$$s = (\hat{\mathbf{b}} \times \hat{\mathbf{n}}) \cdot \nabla \times (\hat{\mathbf{b}} \times \hat{\mathbf{n}}), \tag{3}$$

and satisfies the vector identity [40]

$$s = \frac{\mu_o J_{||}}{B} - 2\tau_n, \tag{4}$$

where τ_n is the normal torsion

$$\tau_n = -\hat{\mathbf{n}} \cdot (\hat{\mathbf{b}} \cdot \nabla)(\hat{\mathbf{b}} \times \hat{\mathbf{n}}). \tag{5}$$

The local shear satisfies

$$s = -\frac{g^{\rho\rho}}{B^2}(\mathbf{B} \cdot \nabla)\frac{\nabla\psi \cdot \nabla\alpha}{g^{\rho\rho}}, \tag{6}$$

where $g^{\rho\rho} = \nabla\rho \cdot \nabla\rho$ and the integrated local shear is given by

$$\Lambda = \frac{g^{\rho\rho}}{B}\int \sqrt{g}d\eta\ s\frac{B^2}{g^{\rho\rho}} = -\frac{\nabla\alpha \cdot \nabla\psi}{B}, \tag{7}$$

where $\sqrt{g} = 1/\mathbf{B} \cdot \nabla\eta = 1/\nabla\psi \times \nabla\alpha \cdot \nabla\eta$ and η labels points along the field line.

In the following, a ballooning ansatz ($k_{||} \ll k_\perp$) is employed where perpendicular wave numbers can be written in general [41]

$$\mathbf{k}_\perp = k_\alpha\nabla\alpha + k_\rho\nabla\rho. \tag{8}$$

The square of the perpendicular wave vector is given by

$$k_\perp^2 = \frac{B^2}{\psi'^2 g^{\rho\rho}}[k_\alpha^2 + (k_\alpha \Lambda - k_\rho \frac{g^{\rho\rho}\psi'}{B})^2]. \tag{9}$$

Additionally, the following quantity enters in the evaluation of the drift frequency

$$\frac{\mathbf{k}\cdot\mathbf{B}\times\vec{\kappa}}{B^2} = \frac{\mathbf{k}\cdot(\kappa_n \hat{\mathbf{b}}\times\hat{\mathbf{n}} - \kappa_g \hat{\mathbf{n}})}{B}$$

$$= \frac{1}{\psi'|\nabla\rho|}[k_\alpha(\kappa_n + \Lambda\kappa_g) - k_\rho \frac{g^{\rho\rho}\psi'}{B}\kappa_g]. \tag{10}$$

Here $\kappa_n + \Lambda\kappa_g$ represents the curvature vector contribution to the toroidal ITG drive in ballooning formalism.

III. THREE FIELD MODEL

A three field model is introduced that describes the evolution of the ion density (n_i), parallel momentum ($v_{||}$) and ion temperature (T_i) for ITG turbulence in the electrostatic limit for 3D geometry. The linearized version of this model has been used in previous microinstability studies of stellarator configurations [20, 42]. As in prior nonlinear ITG studies, $\mathbf{E}\times\mathbf{B}$ advection provides the dominant nonlinearity. In the following, we distinguish between fluctuating quantities with $k_\alpha = 0$ (zonal fields) and fluctuations with $k_\alpha \neq 0$. The non-zonal quantities are governed by the following equations.

$$\frac{\partial n}{\partial t} + \nabla\cdot(n_i\mathbf{v}_E + n_i\mathbf{v}_{i*}) + \nabla\cdot(n_i\mathbf{v}_{pi} + n_i\mathbf{v}_{\pi i})$$

$$+\mathbf{B}\cdot\nabla(n_i\frac{v_{||}}{B}) + \nabla\cdot(n\mathbf{v}_{dis}) = 0, \tag{11}$$

$$m_i n_i \frac{dv_{||}B}{dt} + (\mathbf{B}\cdot\nabla)(n_i e\phi + p_i) + \mathbf{B}\cdot(\nabla\cdot\vec{\vec{\pi}})_{gyro}$$

$$+\mathbf{B}\cdot(\nabla\cdot\vec{\vec{\pi}})_{dis} = 0, \tag{12}$$

$$\frac{3}{2}n_i\frac{dT_i}{dt} + n_i T_i\nabla\cdot\mathbf{v}_i + \nabla\cdot\mathbf{q}_{Di} + \nabla\cdot\mathbf{q}_{dis} = 0, \tag{13}$$

where $d/dt = \partial/\partial t + (\mathbf{v}_E + \mathbf{v}_{i*})\cdot\nabla$. The viscous force $\nabla\cdot\vec{\vec{\pi}}$ is decomposed into gyroviscous and dissipative components. The first of these contributions account for gyroviscous cancellations. The $\mathbf{E}\times\mathbf{B}$ and ion diamagnetic flows are given by

$$\mathbf{v}_E + \mathbf{v}_{i*} = \frac{\mathbf{B}\times\nabla\phi}{B^2} + \frac{\mathbf{B}\times\nabla p_i}{n_i e B^2}, \tag{14}$$

the sum of the ion polarization and gyro-viscosity produce

$$\nabla\cdot(n_i\mathbf{v}_{pi} + n_i\mathbf{v}_{\pi i gyro})$$

$$= -\nabla\cdot[\frac{n_i m_i}{eB^2}(\frac{\partial}{\partial t} + \mathbf{v}_E\cdot\nabla)(\nabla\phi + \frac{1}{n_i e}\nabla p_i)], \tag{15}$$

and the diamagnetic heat flux is given by

$$\mathbf{q}_{Di} = \frac{5}{2}\frac{p_i}{eB^2}\mathbf{B}\times\nabla T_i. \tag{16}$$

The divergences of the $\mathbf{E}\times\mathbf{B}$ and ion diamagnetic flows produce contributions from the curvature vector

$$\nabla\cdot\mathbf{v}_E = \frac{e}{T_i}\mathbf{v}_{Di}\cdot\nabla\phi, \tag{17}$$

$$\nabla\cdot(n_i\mathbf{v}_{*i}) = \frac{1}{T_i}\mathbf{v}_{Di}\cdot\nabla p_i, \tag{18}$$

where

$$\mathbf{v}_{Di} = \frac{2T_i}{eB^2}\mathbf{B}\times\vec{\kappa}, \tag{19}$$

with a low-β approximation $\nabla_\perp B/B \approx \vec{\kappa}$ used. The last terms of Eqs. (11)-(13) account for dissipative physics which are modeled with phenomenological transport coefficients D, $\mu_\perp$ and $\chi_\perp$

$$n_i\mathbf{v}_{dis} = -\frac{\mathbf{B}\times m_i n_i\mu_\perp\nabla^2(\mathbf{v}_E+\mathbf{v}_{i*})}{eB^2} - D\nabla n_i, \tag{20}$$

$$\mathbf{B}\cdot(\nabla\cdot\vec{\vec{\pi}})_{dis} = -nm_i\mu_\perp\nabla^2 v_{||}B, \tag{21}$$

$$\mathbf{q}_{dis} = -n\chi\nabla T_i. \tag{22}$$

Finally, adiabatic electrons are assumed

$$\frac{e\tilde{\phi}}{T_{e0}} = \frac{\tilde{n}}{n_{e0}}. \tag{23}$$

This model is simplified in a number of ways. We consider the ion temperature gradient to be the sole drive for instability and ignore equilibrium gradients in the density $\nabla n_{i0} = 0$. Additionally, we'll assume the fluctuating ion temperature dominates the expression for $\tilde{p}_i$ ($\tilde{T}_i/T_{i0} \gg \tilde{n}_i/n_{i0}$). Formally, this is valid in the more general formulation in the large $\tau = T_e/T_i$ limit while retaining ∇T_{io}. We'll also ignore the $\mathbf{v}_{Di}$ contribution to $\nabla\cdot\mathbf{q}_i$ for simplicity. All fluctuating quantities are written

$$\tilde{\phi} = \sum_{\mathbf{k}}\phi_{\mathbf{k}}e^{i\mathbf{k}_\perp\cdot\mathbf{x}}, \tag{24}$$

where the approximation $k_\perp \gg k_{||}$ is employed with $\mathbf{k}_\perp$ given by Eq. (8).

A set of normalized variables are defined by

$$\frac{e\tilde{\phi}_k}{T_{e0}} = \rho * \Phi_k, \tag{25}$$

$$\frac{\tilde{T}_{ik}}{T_{e0}} = \rho * T_k, \tag{26}$$

$$\frac{v_{||k}}{C_s} = \rho * U_k, \tag{27}$$

where $C_S^2 = T_e/m_i$, $\rho_s = C_s m_i/eB_0$, the dimensionless quantity $\rho*$ is defined

$$\rho* = C_s\frac{m_i}{e\psi'}, \tag{28}$$

and a normalizing magnetic field strength B_0 and equilibrium length scale L_{eq} are introduced. Time is normalized to τ defined by

$$\tau = \frac{L_{eq}}{C_s}, \tag{29}$$

and normalized wave-numbers are denoted

$$k_x = k_\rho \rho * \frac{\psi'}{B_0}, \tag{30}$$

$$k_y = k_\alpha \rho * . \tag{31}$$

Normalized dissipation coefficients are identified

$$\hat{\mu} = \frac{\tau \mu_\perp}{\rho_s^2}, \tag{32}$$

$$\hat{D} = \frac{\tau D}{\rho_s^2}, \tag{33}$$

$$\hat{\chi} = \frac{2\tau \chi_\perp}{3\rho_s^2}. \tag{34}$$

With this, we write the governing equations

$$\frac{\partial}{\partial t}[\Phi_k + B_k(\Phi_k + T_k)] - iD_k(\Phi_k + T_k) + \nabla_{||}\frac{U_k B_0}{B}$$

$$+\hat{D}B_k\Phi_k + \hat{\mu}B_k^2(\Phi_k + T_k)$$

$$= \sum_{k'}(k_x k'_y - k_y k'_x)B_{k'k}\Phi_{k-k'}(\Phi_{k'} + T_{k'}), \tag{35}$$

$$\frac{\partial U_k}{\partial t} + \frac{B_0}{B}\nabla_{||}(\Phi_k + T_k) + \hat{\mu}B_k U_k$$

$$= \sum_{k'}(k_x k'_y - k_y k'_x)\Phi_{k-k'}U_{k'}, \tag{36}$$

$$\frac{\partial T_k}{\partial t} + ik_y\epsilon_T\Phi_k + \hat{\chi}B_k T_k$$

$$= \sum_{k'}(k_x k'_y - k_y k'_x)\Phi_{k-k'}T_{k'}, \tag{37}$$

where $\nabla_{||} = (L_{eq}/B_0)\mathbf{B}\cdot\nabla$ and $\tau\frac{\partial}{\partial t} \rightarrow \frac{\partial}{\partial t}$. The instability drive is due to the ion temperature gradient identified by

$$\epsilon_T = -\frac{L_{eq}}{T_{e0}}\frac{dT_i}{d\rho}, \tag{38}$$

and important geometric quantities are given by

$$D_k = k_y d_y + k_x d_x$$

$$= -k_y\frac{2L_{eq}(\kappa_n + \Lambda\kappa_g)}{|\nabla\rho|} + k_x\frac{2L_{eq}\Lambda_0\kappa_g}{|\nabla\rho|}, \tag{39}$$

$$B_k = k_y^2 b_{yy} - k_x k_y 2b_{xy} + k_x^2 b_{xx}$$

$$= \frac{k_y^2 + (k_y\Lambda - k_x\Lambda_0)^2}{g^{\rho\rho}}, \tag{40}$$

$$B_{k'k} = k'_y k_y b_{yy} - (k'_x k_y + k_x k'_y) b_{xy} + k'_x k_x b_{xx}, \tag{41}$$

$$\Lambda_0 = \frac{g^{\rho\rho} B_0}{B}. \tag{42}$$

The quantity D_k denotes the contribution from the curvature vector and B_k describes $k_\perp^2\rho_s^2$ contributions.

The $k_y = 0$ fluctuations come in two varieties in magnetic confinement devices. Sound wave perturbations driven by geodesic curvature (κ_g) produce geodesic acoustic modes (GAMs). In optimized stellarators, GAMs are generally quickly Landau damped leaving zonal fields (those quantities that are independent of field line) playing the more important role in the nonlinear dynamics. As such, GAM fluctuations are neglected in this model for simplicity. The more important $k_y = 0$ quantities that affect nonlinear saturation physics in the stellarators are zonal fields. As noted earlier, zonal flows physics is more complex in 3D configurations than in 2D devices. Both collisional [43] and collisionless damping mechanisms [30] will be present. In the following, we prescribe a phenomenological zonal flow frequency ω_F to describe its linear properties. Transport coefficients are introduced to denote the linear damping properties of zonal temperature and parallel flow. Following the prescriptions of Refs. [2] and [39], the nonlinear physics of these quantities is given by the associated $\mathbf{E}\times\mathbf{B}$ advection. The governing equations for the $k_y = 0$ fluctuations are given by

$$\frac{\partial \Phi_k^Z}{\partial t} + i\omega_F \Phi_k^Z$$

$$= k_x \sum_{k'} k'_y \Phi_{k-k'} \left(\frac{B_{k'k}}{B_k}\Phi_{k'} + \frac{B_{k'-kk}}{B_k} T_{k'}\right), \tag{43}$$

$$\frac{\partial U_k^Z}{\partial t} + \hat{\mu} b_{xx} k_x^2 U_k^Z = k_x \sum_{k'} k'_y \Phi_{k-k'} U_{k'}, \tag{44}$$

$$\frac{\partial T_k^Z}{\partial t} + \hat{\chi} b_{xx} k_x^2 T_k^Z = k_x \sum_{k'} k'_y \Phi_{k-k'} T_{k'}. \tag{45}$$

Quantities with the superscript Z specifically denote zonal ($k_y = 0$) fluctuations.

One can form an energy-like quantity E given by

$$E = \frac{1}{2}\sum_k \int_{-\infty}^{\infty} \sqrt{g} d\eta [|\Phi_k + T_k|^2 (1 + B_k) + |U_k|^2], \tag{46}$$

where the integral is along the magnetic field line labeled by coordinate η and $\sqrt{g} = 1/\mathbf{B}\cdot\nabla\eta$. An evolution equation for E can be derived and is given by

$$\frac{dE}{dt} - Q\epsilon_T = -\epsilon_{loss}, \tag{47}$$

where Q is the normalized turbulent cross-field heat flux

$$Q = \mathbf{Q}\cdot\nabla\rho = \frac{1}{2}\int_{-\infty}^{\infty} \sqrt{g} d\eta \sum_k i k_y (\Phi_k^* T_k - \Phi_k T_k^*), \tag{48}$$

and ϵ_{loss} is due to dissipative physics

$$\epsilon_{loss} = \sum_k \int_{-\infty}^{\infty} \sqrt{g} d\eta [\hat{\mu}_\perp |B_k|^2 |\Phi_k + T_k|^2 + \hat{\mu}_\perp B_k |U_k|^2$$

$$+ B_k Re(\hat{D}\Phi_k + \hat{\chi} T_k)(\Phi_k^* + T_k^*) + \nu^Z |\Phi_k^Z|^2 \delta_{k_y,0}), \tag{49}$$

where $\hat{\mu}_\perp, \hat{D}$ and $\hat{\chi}$ are normalized transport coefficients and $\nu^Z = -Im(\omega_F)$ denotes the linear zonal flow damping coefficient. In steady state, the energy equation yields the solution for the turbulent heat flux $Q = \epsilon_{loss}/\epsilon_T$. The nonlinearities in our equations conserve E.

IV. LINEAR THEORY

Linear stability theory is carried out in this section. An analysis of the eigenmode equation is made with regard to the special properties of optimized stellarators. In particular, we note that for our three-field model, there are generally three eigenvalues at every choice of $\mathbf{k}$ corresponding to an instability (when the instability condition is satisfied), a nearly complex conjugate stable mode and a nearly marginally stable mode.

Linear eigenmodes with eigenvalue ω are governed by the ordinary differential equation for non-zonal fields along the field line

$$\nabla_{||}(\frac{B_0^2}{B^2}\nabla_{||}\Phi)[1+\frac{k_y\epsilon_T}{\omega}]+\omega^2[1+B_k(1+\frac{k_y\epsilon_T}{\omega})]\Phi$$

$$+D_k\omega[1+\frac{k_y\epsilon_T}{\omega}]=0. \tag{50}$$

In deriving this formula, dissipative terms are dropped but can be easily included. For a 3D equilibrium, this equation generally requires a numerical solution for precise predictions for growth rates and eigenmode structure of the most unstable mode at each choice of k_x and k_y. With knowledge of the mode structure along the field line, one can define a eigenmode average of various geometric quantities for the most unstable mode defined by

$$< A >_0 = \frac{\int_{-\infty}^{\infty}\sqrt{g}d\eta A|\Phi|^2}{\int_{-\infty}^{\infty}\sqrt{g}d\eta|\Phi|^2}. \tag{51}$$

Similarly, we define the average parallel mode number via

$$< k_{||}^2 >_0 = \frac{\int_{-\infty}^{\infty}\sqrt{g}d\eta|\frac{B_0}{B}\nabla_{||}\Phi|^2}{\int_{-\infty}^{\infty}\sqrt{g}d\eta|\Phi|^2}. \tag{52}$$

The parallel mode structure is sensitive to the properties of the local shear. In stellarator configurations, the local shear (s) varies considerably within a magnetic surface. The local shear as a function of distance along the field line label is typically characterized by relatively long regions where s has a small negative ('tokamak'-like) value and localized regions with large positive ('stellarator'-like) value as the field line passes through ridges or corners on the flux surface. The average magnetic shear $d\iota/d\rho$ is computed by an appropriate average of the local shear. Because of the 'bumps' present in the local shear, the integrated local shear experiences jumps as it passes through these regions that produce a localizing potential and dictates an effective $k_{||}$ for the eigenmode. See Appendix A for further discussion of this point.

Using the notation defined in Eqs. (51) and (52), an expression for ω can be derived for a given magnetic geometry given by

$$\omega^3(1+< B_k >_0)+\omega^2(< B_k >_0 k_y\epsilon_T+< D_k >_0)+$$

$$\omega(< D_k >_0 k_2\epsilon_T- < k_{||}^2 >_0)- < k_{||}^2 >_0 k_y\epsilon_T=0. \tag{53}$$

When $A^3/27+C^2/4>0$, there are three roots of the form

$$\omega_i=-\frac{\alpha}{3}+e^{i\theta_i}[\frac{C}{2}+\sqrt{\frac{A^3}{27}+\frac{C^2}{4}}]^{1/3}$$

$$-e^{-i\theta_i}[-\frac{C}{2}+\sqrt{\frac{A^3}{27}+\frac{C^2}{4}}]^{1/3}, \tag{54}$$

where

$$A=\beta-\frac{\alpha^2}{3}, \tag{55}$$

$$C=\lambda+\frac{\alpha\beta}{3}-\frac{2\alpha^3}{27}, \tag{56}$$

$$\alpha = \frac{< D_k >_0 + k_y \epsilon_T < B_k >_0}{1 + < B_k >_0}, \tag{57}$$

$$\beta = \frac{k_y \epsilon_T < D_k >_0 - < k_{||}^2 >_0}{1 + < B_k >_0}, \tag{58}$$

$$\lambda = \frac{k_y \epsilon_T < k_{||}^2 >_0}{1 + < B_k >_0}. \tag{59}$$

and $e^{3i\theta} = 1$. The choice $\theta = 2\pi/3$ yields a growing mode (denoted ω_1 in the following), $\theta = -2\pi/3$ produces a complex conjugate ($\omega_2 = \omega_1^*$) damped mode and $\theta = 0$ produces a marginally stable mode (denoted ω_3). When $A^3/27 + C^2/4 < 0$, only real roots are present with no instability. For a given k_x, instabilities are only present in a finite range in k_y corresponding to $k_{crit1} < k_y < k_{crit2}$.

In deriving these expressions, dissipation terms are dropped. In reality, dissipative processes are present and provide energy sinks for the turbulence. Dissipative effects can be easily included in the linear analysus in the special case $\hat{\mu} = \hat{D} = \hat{\chi}$ which effectively modifies the eigenfrequencies to be

$$\omega_p \rightarrow \omega_p - i < B_k >_0 \hat{\mu}, \tag{60}$$

In this model, dissipation adds a damping term that scales with $k_\perp^2$. With finite dissipation, ω_1 and ω_2 are only approximately complex conjugates $\omega_2 - \omega_1^* \approx -2i < B_k >_0 \hat{\mu}$ and the third eigenmode is weakly damped.

In this model, ITG instability comes in two varieties [44]. The toroidal ITG branch is determined by the magnetic curvature properties and is crudely described by the relation $\omega^2 \approx -k_y \epsilon_T < D_k >_0$. This expression is essentially the linear ITG instability proxy used in the optimization studies of Refs. [13] and [14]. In this limit, due to the curvature drive of the mode the growth rate will be strongly k_x dependent even at long wavelength. The 'slab'-like branch is due to finite $k_{||}$ and is approximately given by the balance $\omega^3 \approx k_y \epsilon_T < k_{||}^2 >_0$. A property of the slab-ITG eigenvalues is that growth rates are only unstable in a band of wave numbers. Instability only occurs for $k_{crit1} < k_y < k_{crit2}$ where $k_{crit1}^2 \sim 4 < k_{||}^2 >_0 / (27\epsilon_T^2)$ (in the 'weak' D_k limit) and is weakly a function of k_x while $k_{crit2}^2 \sim 27 < k_{||}^2 >_0 / (4\epsilon_T^2 < b_{22} >_0^3)$ at $k_x = 0$. However, k_{crit2} is a strong function of k_x. In practice, instabilities can occur for $k_y < k_{crit1}$. At long wavelength, the eigenmodes become extended along the field line and a different theoretical treatment is required. This is discussed further in Appendix A.

Roughly, the slab-like solution dominates when

$$< k_{||}^2 >_0^{1/2} \gtrsim k_y^{1/4} \epsilon_T^{1/4} < D_k >_0^{3/4}. \tag{61}$$

For configurations like the tokamak, that have relatively long parallel wavelengths ($k_{||} \sim 1/qR$ for major radius R and safety factor $q = 1/\iota$), the toroidal ITG branch is dominant, whereas configurations such as quasi-helically symmetric stellarators with considerably smaller parallel wavelengths ($k_{||} \sim |N - \iota|/R$ for an N-period QHS), the slab-like branch dominates.

For each eigenvalue, there is an associated eigenvector. To assist in the eigenvector identification, we introduce the quantity G_k which serves as a potential function for U_k

$$U_k = \frac{B_0}{B} \nabla_{||} G_k. \tag{62}$$

Using this notation, the governing equations can be rewritten in the form

$$(1 + < B_k >_0) \frac{\partial \Phi_k}{\partial t} - i(< D_k >_0 + k_y \epsilon_T < B_k >_0) \Phi_k$$

$$-i < D_k >_0 T_k - < k_{||}^2 >_0 G_k + \hat{\mu} [< B_k > + < B_k^2 >] \Phi_k$$

$$= \sum_{k'} (k_x k_y' - k_y k_x') \{ \Phi_{k-k'} (B_{k'k} \Phi_{k'} + B_{k'-kk} T_{k'}) \}, \tag{63}$$

$$\frac{\partial G_k}{\partial t} + \Phi_k + T_k + \int_{-\infty}^{\eta} \sqrt{g} d\eta \hat{\mu} B_k \nabla_{||} G_k$$

$$= \sum_{k'} (k_x k'_y - k_y k'_x) \int_{-\infty}^{\eta} \sqrt{g} d\eta \Phi_{k-k'} \nabla_{||} G_{k'}, \tag{64}$$

$$\frac{\partial T_k}{\partial t} + i k_y \epsilon_T \Phi_k + \hat{\mu} B_k T_k = \sum_{k'} (k_x k'_y - k_y k'_x) \Phi_{k-k'} T_{k'}, \tag{65}$$

where the $\{...\}$ operator denotes

$$\{\Phi_{k-k'}(B_{k'k}\Phi_{k'} + B_{k'-kk}T_{k'})\}$$

$$= \Phi_k \frac{\int \sqrt{g} d\eta \Phi^*_k \Phi_{k-k'}(B_{k'k}\Phi_{k'} + B_{k'-kk}T_{k'})}{\int \sqrt{g} d\eta |\Phi_k|^2}$$

$$= \{B_{k'k}\}_0 \Phi_{k-k'} \Phi_{k'} + \{B_{k'-kk}\}_0 \Phi_{k-k'} T_{k'}. \tag{66}$$

In this form, the fluid variables still retain their dependence on field line label η.

For non-zonal quantities, the evolution equations can be rewritten by expressing the fields in terms of the eigenmode expansion. There is a linear relationship between the fluid variables $\vec{\Phi_k} = (\Phi_k, T_k, G_k)^T$ and the linear eigenmodes $\vec{\beta} = (\beta_1, \beta_2, \beta_3)^T$ by the definition $\vec{\Phi_k} = M_k \vec{\beta}$, $\vec{\beta} = M_k^{-1} \vec{\Phi_k}$ [$\Phi_p = m_{pq}\beta_q, \beta_p = m^{-1}_{pq}\phi_q$ $m_{pq}(k) = m_{pq}, m_{pq}(k') = m'_{pq}, m_{pq}(k-k') = m''_{pq}$]. Expressions for the matrix M_k and its inverse are given in Appendix B. The components of the vector $\vec{\beta}$ satisfy

$$\frac{\partial \beta_p}{\partial t} + i\omega_p \beta_p$$

$$= m^{-1}_{p1} \sum_{k'} \frac{(k_x k'_y - k_y k'_x)}{1 + < B_k >_0} \{\Phi_{k-k'}(B_{k'k}\Phi_{k'} + B_{k'-kk}T_{k'})\}$$

$$+ m^{-1}_{p2} \sum_{k'} (k_x k'_y - k_y k'_x) \{\Phi_{k-k'} T_{k'}\}$$

$$+ m^{-1}_{p3} \sum_{k'} (k_x k'_y - k_y k'_x) \{\int_{-\infty}^{\eta} \sqrt{g} d\eta \Phi_{k-k'} \nabla_{||} G_{k'}\}. \tag{67}$$

These equations apply to the eigenmodes for the non-zonal ($k_y \neq 0$) fields. As written in Eqs. (43)-(45), the three linear eigenmodes of the zonal fields are simply the basic fields Φ^Z_k, U^Z_k and T^Z_k corresponding to the eigenvalues ω_F, $(-i\hat{\mu} b_{xx} k_x^2)$ and $(-i\hat{\chi} b_{xx} k_x^2)$, respectively. With this identification, we can rewrite the nonlinear contribution to Eq. (67) by segregating out contributions from coupling to zonal fields due to $k'_y = 0$ and $k_y = k'_y$. Using $\vec{\Phi_k} = M_k \vec{\beta}$, these expressions are given by

$$\frac{\partial \beta_p}{\partial t} + i\omega_p \beta_p = \sum_{k'_x (k_y = k'_y)} C_{pqF} \Phi^Z_{k-k'} \beta'_q$$

$$+ \sum_{k'_x (k'_y = 0)} C_{pFq} \Phi^Z_{k'} \beta''_q + \sum_{k'_x (k'_y = 0)} C_{pTq} T^Z_{k'} \beta''_q$$

$$+ \sum_{k'_x (k'_y = 0)} \int_{-\infty}^{\eta} \sqrt{g} d\eta C_{pUq} U^Z_{k'} \beta''_q + {\sum_{k'}}' C_{pqr} \beta'_q \beta''_r$$

$$+\sum_{k'}{}' \int_{-\infty}^{\eta} \sqrt{g} d\eta \overline{C}_{pqr} (\beta''_r \nabla_{||} \beta'_q - \beta'_q \nabla_{||} \beta''_r), \tag{68}$$

where the sums with primes ($\sum'_{k'}$) exclude $k'_y = 0$ and $k'_y = k_y$ with $\beta'_q = \beta_q(k')$ and $\beta''_r = \beta_r(k - k')$. The Einstein convention is used to imply sums over repeated indices q, r and the matrix coefficients are defined by

$$C_{pqF} = k_y (k_x - k'_x)[m_{p1}^{-1} \frac{\{B_{k'k}\}_0 m'_{1q} + \{B_{k'-kk}\}_0 m'_{2q}}{1 + < B_k >_0}$$

$$+ m_{p2}^{-1} m'_{2q} + m_{p3}^{-1} m'_{3q}] \tag{69}$$

$$C_{pFq} = -k_y k'_x \frac{m_{p1}^{-1} \{B_{k'k}\}_0 m''_{1q}}{1 + < B_k >_0}, \tag{70}$$

$$C_{pTq} = -k_y k'_x (\frac{m_{p1}^{-1} \{B_{k'-kk}\}_0 m''_{1q}}{1 + < B_k >_0} + m_{p2}^{-1} m''_{1q}), \tag{71}$$

$$C_{pUq} = -k_y k'_x m_{p3}^{-1} m''_{1q}, \tag{72}$$

$$C_{pqr} = (k_x k'_y - k_y k'_x)[\frac{m_{p1}^{-1} m''_{1r} (\{B_{k'k}\}_0 m'_{1q} + \{B_{k'-kk}\}_0 m'_{2q})}{1 + < B_k >_0}$$

$$+ m_{p2}^{-1} m''_{1r} m'_{2q} + \frac{1}{2} m_{p3}^{-1} m''_{1r} m'_{3q}], \tag{73}$$

$$\overline{C}_{pqr} = \frac{1}{2} (k_x k'_y - k_y k'_x) m_{p3}^{-1} m'_{3q} m''_{1r}, \tag{74}$$

with $m'_{ij} = m_{ij}(k')$ and $m''_{ij} = m_{ij}(k - k')$. The equivalent expressions for the zonal fields are

$$\frac{\partial \Phi_k^Z}{\partial t} + i\omega_F \Phi_k^Z = \sum_{k'} C_{Fqr} \beta'_q \beta''_r, \tag{75}$$

$$\frac{\partial U_k^Z}{\partial t} + \hat{\mu} b_{xx} k_x^2 U_k^Z = \sum_{k'} k_x k'_y m''_{1r} \beta''_r \nabla_{||} (m'_{3q} \beta'_q), \tag{76}$$

$$\frac{\partial T_k^Z}{\partial t} + \chi b_{xx} k_x^2 T_k = \sum_{k'} k_x k'_y m''_{1r} m'_{2q} \beta'_q \beta''_r, \tag{77}$$

where

$$C_{Fqr} = k_x k'_y m''_{1r} (\frac{B_{k'k}}{B_k} m'_{1q} + \frac{B_{k'-kk}}{B_k} m'_{2q}). \tag{78}$$

The turbulent heat flux Q can also be re-expressed in terms of the eigenmode expansion. Using the expressions for the three eigenfrequencies $\omega_1 = \omega_R + i\gamma, \omega_2 = \omega_R - i\gamma, \omega_3 = Re(\omega_3)$ from Eq. (54) and Eq. (48), one derives

$$Q = \int_{-\infty}^{\infty} \sqrt{g} d\eta \sum_k \frac{k_y^2}{|\omega_1|^2} \epsilon_T \{\gamma[|\beta_1|^2 - |\beta_2|^2$$

$$+Re(\beta_3\beta_1^*) - Re(\beta_3\beta_2^*)]$$

$$+(\frac{|\omega_1|^2}{\omega_3} - \omega_R)[Im(\beta_1\beta_3^*) + Im(\beta_2\beta_3^*)]\}. \quad (79)$$

The leading term in this equation corresponds to the contribution to quasi-linear transport driven by the unstable eigenmode. However, we see from this expression that if energy can be transferred from the unstable eigenmodes into stable modes, non-trivial corrections to quasilinear theory can be realized. In order to deduce relationships between different contributions to Q, use examine the nonlinear transfer physics in the following section and deduce turbulent saturation amplitudes.

A distinguishing feature of the fluid theory employed here for ITG turbulent saturation is the use of three fields instead of the two-field model employed in Refs. [2, 3, 38, 39]. The three-field model allows a description of the slab-like ITG branch and contains three eigenfrequencies (and associated eigenmodes) at each wavenumber. While the two-field model does describe the toroidal-ITG branch, it does not allow for a marginally stable mode (ω_3) and hence its presence is precluded from playing any role in nonlinear saturation. However, as discussed in the subsequent section, nonlinear saturation for toroidal ITG turbulence is dominated by a three-wave interaction involving an unstable mode (ω_1), a damped mode (ω_2) and a zonal mode. As the two-field model is predominantly used as a model for ITG turbulent saturation in tokamaks where the toroidal ITG branch dominates, neglect of ω_3 in turbulent saturation physics is a reasonable approximation. However, this approximation is not be generally justified for ITG saturation physics in stellarators with slab-like ITG eigenmodes.

V. NONLINEAR ENERGY TRANSFER

In the previous section, we developed a model for ITG turbulence based on a three-field fluid formulation and discussed aspects of the associated linear theory. In particular, an eigenmode decomposition was utilized that distinguishes between three classes of non-zonal modes, linear instabilities, damped modes and nearly marginally stable modes. In the following section, we concentrate on the nonlinear evolution of the turbulence with an eye towards deriving a turbulent saturation theory.

As noted in Eq. (68), nonlinearities in the theory come in two varieties, those involving zonal fields and those that do not. In the following we develop two cases assuming one of these classes of nonlinearities dominates nonlinear energy transfer. For turbulence associated with ITG modes of the toroidal variety (as in tokamaks), prior studies have indicated that nonlinearities involving zonal flows dominate [1–3]. In this case, we will find that the saturation physics is effectively mediated by the zonal flows that transfer energy from the unstable modes to the stable modes. However, nonlinear energy transfer involving purely non-zonal eigenmodes can also provide an energy transfer channel. In fact, our calculations indicate that for quasi-helically symmetric configurations (as embodied by HSX), coupling between unstable and damped eigenmodes may be mediated by a three wave interaction involving the marginally stable eigenmode. We will develop the theory for these two sub-cases in the following sections.

In order to obtain information on turbulent saturation, we rely on statistical arguments and turbulence closure theories. A bracket notation is introduced to describe an ensemble average. Using this and Eq. (68), an evolution equation for quadratic quantities can be derived given by

$$\frac{\partial}{\partial t} < |\beta_p|^2 > -2Im(\omega_p) < |\beta_p|^2 >=$$

$$= 2Re[\sum_{k'_x(k_y=k'_y)} C_{pqF} < \beta_p^* \Phi^Z_{k-k'} \beta'_q >]$$

$$+2Re[\sum_{k'_x(k'_y=0)} C_{pFq} < \beta_p^* \Phi^Z_{k'} \beta''_q >]$$

$$+2Re[\sum_{k'_x(y'_2=0)} C_{pTq} < \beta_p^* T^Z_{k'} \beta''_q >]$$

$$+2Re[\sum_{k'_x(y'_2=0)} < \beta_p^* \int_{-\infty}^{\eta} \sqrt{g} d\eta C_{pUq} U^Z_{k'} \beta''_q >]$$

$$+2Re[\sum_{k'}{}' < \beta_p^* \int_{-\infty}^{\eta} \sqrt{g} d\eta \overline{C}_{pqr} (\beta''_r \nabla_{||} \beta'_q - \beta'_q \nabla_{||} \beta''_r) >]$$

$$+2Re[\sum_{k'}{}' C_{pqr} < \beta_p^* \beta'_q \beta''_r >]. \tag{80}$$

In this form, we see the evolution of the quadratic quantities requires a closure for quantities that contain third order fluctuations.

A. Zonal flow mediated saturation

For the case that zonal flow nonlinearities dominate the nonlinear transfer, the mode evolution for mode β_p is given by the approximate expression [45]

$$\frac{\partial \beta_p}{\partial t} + i\omega_p \beta_p \approx \sum_{k'_x(k_y=k'_y)} C_{pqF} \Phi^Z_{k-k'} \beta'_q. \tag{81}$$

The corresponding evolution equation for the energy density in mode β_p is given by the approximate equation

$$\frac{\partial}{\partial t} < |\beta_p|^2 > -2Im(\omega_p) < |\beta_p|^2 >$$

$$\approx 2Re[\sum_{k'_x(k_y=k'_y)} C_{pqF} < \beta_p^* \Phi^Z_{k-k'} \beta'_q >], \tag{82}$$

Here, we are interested in low-k dynamics, in which case, we neglect the second terms in Eq. (68) relative to the first term, noting $C_{pFq}/C_{pqF} \sim k^2$ at small k. To make further progress, a theory for the triplet correlation function $< \beta_p^* \Phi^Z_{k-k'} \beta_q >$ is needed. To accomplish this, we follow the procedure of [2] and derive expressions for the time derivative of the triple product. Using $d/dt < \beta_p^* \beta_q \Phi^Z_{k-k'} >=< \beta_q \Phi^Z_{k-k'} d\beta_p^*/dt > + < \beta_p^* \Phi^Z_{k-k'} d\beta_q/dt > + < \beta_p^* \beta_q d\Phi^Z_{k-k'}/dt >$ and the evolution equations for β_p and Φ^Z, Eqs. (68) and (75), one derives

$$[\frac{d}{dt} + i(\omega''_F + \omega'_q - \omega_p^*)] < \beta_p^* \Phi^Z_{k-k'} \beta_q >= \mathcal{G}, \tag{83}$$

where $\mathcal{G}$ is due to nonlinear contributions from each evolution equation and is proportional to quartic correlations. In order to make analytic progress, we implement an eddy damped quasi-normal Markovian (EDQNM) closure argument to write $\mathcal{G}$ in terms of lower order correlation moments. Part of $\mathcal{G}$ is proportional to $< \beta_p^* \Phi_{k-k'} \beta_q >$ and hence effectively renormalizes the complex frequency to

$$\hat{\omega}''_F + \hat{\omega}'_q - \hat{\omega}_p^* = \omega''_F + \omega'_q - \omega_p^* + \Delta\omega''_F + \Delta\omega'_q - \Delta\omega_p^*, \tag{84}$$

where $\Delta\omega$ denotes an amplitude-dependent correction to the linear eigenfrequency. We provide formulae for $\Delta\omega$ in Appendix C. The remaining part of $\mathcal{G}$ can be expressed as the products of two quadratic correlations. In the time-asymptotic steady-state limit, the solution to Eq. (83) is given by

$$< \beta_p^* \Phi^Z_{k-k'} \beta_q >= \tau_{pqF} \sum_r < |\Phi^Z_{k-k'}|^2 > \hat{C}^F_{pq}, \tag{85}$$

where

$$\hat{C}^F_{pq} = C^*_{prF} < \beta'_q \beta'^*_r > - C'_{qrF} < \beta_r \beta_p^* >, \tag{86}$$

$C'_{qrF} = -C_{qrF}(k',k)$ and

$$\tau_{pqF} = \frac{1}{i[\hat{\omega}''_F + \hat{\omega}'_q - \hat{\omega}^*_p]}. \tag{87}$$

The quantity τ_{pqF} plays an important role in the nonlinear saturation physics described here. It can be interpreted as the turbulent correlation time, as it indicates the time over which the three modes interact. Larger values of τ_{pqF} indicate larger nonlinear transfer rates and correspondingly smaller turbulent transport levels are acheivable for a given instability drive. As discussed later, adjusting the magnetic geometry to maximize the turbulent correlation lifetime in stellarator optimization schemes can provide a mechanism to reduce turbulent transport.

At long wavelength, the nonlinear contributions ($\sim \Delta\omega$) to τ_{pqF} are relatively small. Hence, at small k, where the bulk of the turbulent transport occurs, using the linear eigenmode frequencies in evaluating τ_{pqF} is a sensible approximation. In practice, only a few particular choices for p and q yield large values of τ_{pqF} demonstrating that there are preferred channels for nonlinear energy transfer. For the important case $p = 1$, corresponding to nonlinear energy transfer rate out of the unstable eigenmode, τ_{12F} tends to have the largest value when the zonal flow frequency is small (as might be expected in a neoclassical optimized stellarator). From the expression $(\tau_{12F})^{-1} = i[\omega_F(\Delta k_x) + \omega_2(k_x - \Delta k_x, k_y) - \omega_1^*(k_x, k_y)]$ and the property $\omega_1^*(k_x, k_y) \approx \omega_2(k_x, k_y)$ we see that τ_{12F} can be large if ω_F is sufficiently small and that ω_1 is weakly a function of k_x, which tends to be case at small k_y (particularly if the eigenmodes are more 'slab-like'). In this case, the dominant nonlinear energy transfer is from unstable eigenmodes to stable eigenmodes at comparable wavelength with the energy exchange mediated by the zonal flow. This is the dominant nonlinear energy transfer process in tokamak geometry [2].

Using Eqs. (82) and (85), an equation for the evolution of the energy density of mode β_p is derived

$$\frac{\partial}{\partial t} < |\beta_p|^2 > -2Im(\omega_p) < |\beta_p|^2 >$$

$$\approx 2Re[\sum_{k'_x(k_y=k'_y)qr} \tau_{pqF} C_{pqF} < |\Phi^Z_{k-k'}|^2 > \hat{C}^F_{pq}]. \tag{88}$$

Following a similar procedure, one can derive expressions for the evolution of the set of quadratic quantities $< \beta_p \beta_s^* >$. These are given by

$$\frac{\partial}{\partial t} < \beta_p \beta_s^* > = i(\omega_s^* - \omega_p) < \beta_p \beta_s^* >$$

$$+ \sum_{k'q} \tau_{sqF} C_{pqF} \sum_u C^*_{suF} < \beta'^*_u \beta'_q > < |\Phi_{k-k'}|^2 >$$

$$- \sum_{k'q} \tau_{sqF} C_{pqF} \sum_u C'_{quF} < \beta^*_s \beta_u > < |\Phi_{k-k'}|^2 >$$

$$+ \sum_{k'q} \tau^*_{pqF} C^*_{sqF} \sum_u C_{puF} < \beta'_u \beta'^*_q > < |\Phi_{k-k'}|^2 >$$

$$- \sum_{k'q} \tau^*_{pqF} C^*_{sqF} \sum_u C'^*_{quF} < \beta_p \beta^*_u > < |\Phi_{k-k'}|^2 > . \tag{89}$$

From these expressions, we find that the renormalization procedure allows one to write the nonlinearity as the product of a quadratic quantities $< \beta_i \beta_j^* >$ and the energy density associated with the zonal flows.

In steady state, the solution to Eq. (89) can be written in a matrix form $\sum_j D_{ij} E_j = 0$ where E is column vector associated with the quadratic quantities

$$E = \begin{pmatrix} < |\beta_1|^2 > \\ < |\beta_2|^2 > \\ < \beta_1 \beta_2^* > \\ < \beta_2 \beta_1^* > \\ < \beta_1 \beta_3^* > \\ < \beta_1^* \beta_3 > \\ < \beta_2 \beta_3^* > \\ < \beta_2^* \beta_3 > \\ < |\beta_3|^2 > \end{pmatrix}, \tag{90}$$

and D can be constructed as the sum of two matrices $D = D_0 + D_1$. The matrix $(D_0)_{ij} = d_i\delta_{ij}$ is diagonal whose entries are given by linear eigenfrequencies with $d_1 = -d_2 = 2\gamma, d_3 = d_4 = d_9 = 0, d_5 = -d_8 = \gamma_\Delta, d_6 = -d_7 = \gamma_\Delta^*$ where $\omega_1 = \omega_2^* = \omega_R + i\gamma$ and $\gamma_\Delta = \gamma + i(\omega_3 - \omega_R)$. D_1 is a dense matrix with each entry given as the sum over k' of quantities that involve the product of turbulent correlation times, two coupling coefficients, $< |\Phi^Z_{k-k'}|^2 >$ and for some entries the ratio of spectral quantities $< \beta_i'\beta_j'^* > / < \beta_i\beta_j^* >$.

Solutions to $\sum_j D_{ij}E_j = 0$ requires $det|D| = 0$. This condition can be interpreted as a generalized eigenvalue condition for the amplitude of the zonal flows [45]. While a precise value for the zonal flow amplitudes depends upon the details of the coupling coefficients, this level can be roughly approximated with the expression $< |\Phi^Z_{k-k'}|^2 > \sim \gamma/\tau C^2$. In the limit that the dominant nonlinear saturation mechanism is the transfer of energy from unstable to damped modes, a more precise estimate is given by

$$< |\Phi^Z_{k-k'}|^2 > \sim \frac{\gamma}{\tau_{12F} C_{12F} C}. \tag{91}$$

Assuming that at least one of the generalized eigenvalues yields physical answers, the associated eigenvector can be used to deduce relationships between different components of the vector E. In particular, nontrivial solutions to $\sum_j D_{ij}E_j = 0$ yields

$$E = \begin{pmatrix} < |\beta_1|^2 > \\ < |\beta_2|^2 > \\ < \beta_1\beta_2^* > \\ < \beta_2\beta_1^* > \\ < \beta_1\beta_3^* > \\ < \beta_1^*\beta_3 > \\ < \beta_2\beta_3^* > \\ < \beta_2^*\beta^3 > \\ < |\beta_3|^2 > \end{pmatrix} =< |\beta_1|^2 > \begin{pmatrix} 1 \\ f_2 \\ f_3 \\ f_4 \\ f_5 \\ f_6 \\ f_7 \\ f_8 \\ f_9 \end{pmatrix} \tag{92}$$

The turbulent heat flux expression Eq. (79) can be rewritten

$$Q = \int_{-\infty}^{\infty} \sqrt{g} d\eta \sum_k k_2^2 \epsilon_T \frac{\gamma}{|\omega_1|^2} [g_1|\beta_1|^2 + g_2|\beta_2|^2$$

$$+ g_5\beta_1\beta_3^* + g_6\beta_1^*\beta_3 + g_7\beta_2\beta_3^* + g_8\beta_2^*\beta_3], \tag{93}$$

where $g_1 = 1, g_2 = -1, g_5 = (1 - i\delta)/2, g_6 = (1 + i\delta)/2, g_7 = (-1 - i\delta)/2. g_8 = (-1 + i\delta)/2$ and $\delta = (|\omega_1|^2 - \omega_3\omega_3)/\gamma\omega_3$ Using the above expression for the eigenvector, we have

$$Q = \int_{-\infty}^{\infty} \sqrt{g} d\eta \sum_k k_2^2 \epsilon_T \frac{\gamma}{|\omega_1|^2} |\beta_1|^2 \sum_{i=1}^{i=9} f_i g_i. \tag{94}$$

with $f_1 = 1$ and $g_3 = g_4 = g_9 = 0$. As this procedure allows us to find relationships between different quadratic quantities, we are able to relate the heat flux to the amplitude of the turbulence level.

Following the same procedure for the zonal flow equation [Eq. (75)], one derives the following evolution equation for the zonal flow energy at wavenumber k

$$\frac{\partial}{\partial t} < |\Phi^Z_k|^2 > = -2\nu^Z < |\Phi^Z_k|^2 >$$

$$+ 2Re \sum_{k'} C^*_{Fqr} < \Phi^Z_k \beta_q'^* \beta_r''^* >, \tag{95}$$

where $\nu^Z = -\Im(\omega_F)$ is the linear zonal flow damping rate. This equation represents a balance of zonal flow generation from the turbulence and linear damping properties of the zonal flow. Using the turbulent closure relation derived previously to calculate $< \Phi^Z_k \beta_q'^* \beta_r''^* >$, one obtains

$$\frac{\partial}{\partial t} < |\Phi^Z_k|^2 > = -2\nu^Z < |\Phi^Z_k|^2 >$$

$$+2Re\sum_{k'qr}\tau_{qrF}(k',-k'')C^*_{Fqr}<|\Phi^Z_k|^2>\times$$

$$\sum_s[C^*_{qsF}(k',-k'')<\beta''^*_r\beta''_s>-C'_{rsF}(k',-k'')<\beta'^*_q\beta'_s>]. \tag{96}$$

As discussed ealier, in practice only a few choices for τ_{qrF} produce large contributions.

Steady state solutions to Eq. (96) balance the turbulent drives and damping against linear zonal flow damping physics. In the limit of large zonal flow damping from either collisional [43] or collisionless [30] mechanisms, this equation yields a simple estimate for the zonal flow saturated state. In this limit, the zonal flow amplitude cancels out of the evolution equation and one is left with an equation that only involves quadratic quantities involving turbulent fields. Steady state solutions to Eq. (96) can be written

$$2\nu^Z=\sum_i h_i E_i, \tag{97}$$

where $E_i\sim<\beta_j\beta^*_k>$ are components of the column vector E of quadratic quantities given in Eq. (90) and the element h_i are sums over k' of quantities that are the product of turbulent correlation times, two coupling coefficients and the ratio of spectral quantities $<\beta'_i\beta'^*_j>/<\beta_i\beta^*_j>$ and $<\beta''_i\beta''^*_j>/<\beta_i\beta^*_j>$. Using Eq. (92) to relate components of E, the saturated amplitude of the turbulence is predicted to be

$$<|\beta_1|^2>=\frac{2\nu^Z}{\sum_{i=1}^{i=9}f_ih_i}. \tag{98}$$

In this limit, the saturation physics is defined by a balance of zonal flow generation as described by a three-wave interaction involving unstable and damped eigenmodes and the zonal flow and large linear damping of zonal flows. The degree of nonlinear generation is quantified by geometric coupling coefficients and the turbulent correlation times τ_{pqF}. In steady-state, this balance provides a prediction for the turbulence level given by $<|\beta_1|^2>\sim\nu^F/\tau_{pqF}C^2$. Inserting the above solution into the expression for the Q [Eq. (94)], one derives a prediction for the turbulent transport

$$Q=\int_{-\infty}^{\infty}\sqrt{g}d\eta\sum_k k_2^2\epsilon_T\frac{2\gamma\nu^Z}{|\omega_1|^2}\frac{\sum_{i=1}^{i=9}f_ig_i}{\sum_{i=1}^{i=9}f_ih_i}. \tag{99}$$

If the f_1 contribution dominates the sums, the heat flux is approximately given by

$$Q=\int_{-\infty}^{\infty}\sqrt{g}d\eta\sum_k k_2^2\epsilon_T\frac{\gamma}{|\omega_1|^2}\frac{2\nu^Z}{h_1}$$

$$\sim\frac{\gamma\nu^Z}{|\omega_1|^2(C^*_{F21}C^*_{21F}\tau_{21F}-C^*_{F12}C'_{21F}\tau_{12F})}, \tag{100}$$

where the last expression assumes the prevalence of zonal flows mediating the transfer of energy from unstable to damped modes as the dominant nonlinear transfer process.

In high-performance neoclassically-optimized stellarators where linear zonal flow damping is weak, turbulent saturation is more complicated. In this limit, amplitude-dependent complex frequency corrections dominate the linear zonal flow physics. Importantly, as shown in Eq. (84), these amplitude dependent frequency corrections enter into expressions for the turbulent correlation times. Details for how to calculate these corrections are given in Appendix C. With weak linear damping, the saturated solution to the zonal flow evolution equation requires a subtle accounting of the zonal flow drives and damping produced by the turbulence. Since the nonlinear frequency shifts play a larger role at higher k, in some cases turbulence-induced drives for zonal flow are segregated from turbulence induced damping of zonal flows in k space [46]. While the weak linear zonal damping limit is of more relevance to modern day optimized stellarators, we do not pursue this case further here and leave this important limit for future work .

B. Non-zonal mode mediated saturation

In this section, we generalize the saturation theory of the previous section to include non-zonal contributions to turbulent saturation. While zonal flows are known to play an important role in the ITG saturation physics in tokamaks,

there are other nonlinear transfer channels that can accommodate turbulent saturation. In this case, the dominant three-wave interaction associated with the transfer of energy from unstable to damped modes is mediated by a nearly marginally stable non-zonal field (ω_3 in the notation of this calculation). For this case, the relevant evolution equation for mode p is given by

$$\frac{\partial \beta_p}{\partial t} + i\omega_p \beta \approx \sum_{k'}{}' C_{pqr} \beta'_q \beta''_r. \tag{101}$$

In the summation $\sum'_{k'}$, contributions from $k'_y = 0$ and $k'_y = k_y$ are excluded as they account for zonal field contributions. From Eq. (102), one can derive the evolution equation for quadratic quantities

$$\frac{\partial}{\partial t} < \beta^*_q \beta_p >= i(\omega^*_q - \omega_p) < \beta^*_q \beta_p >$$

$$+ \sum_{k'}{}' (C_{pst} < \beta^*_q \beta'_s \beta''_t > + C^*_{qst} < \beta_p \beta'^*_s \beta''^*_t >). \tag{102}$$

Following the procedure from the last section, an evolution equation for the third order quantity can be derived from $d/dt < \beta^*_q \beta'_s \beta''_t >=< \beta'_s \beta''_t d\beta^*_q/dt > + < \beta^*_q \beta''_t d\beta'_s/dt > + < \beta^*_q \beta'_s d\beta''_t/dt >$ and Eq. (102). This produces an equation of the form

$$[\frac{d}{dt} + i(\omega''_t + \omega'_s - \omega^*_q)] < \beta^*_q \beta'_s \beta''_t >= \mathcal{G}_0, \tag{103}$$

where as in Eq. (83), $\mathcal{G}_0$ results from the nonlinear contributions from each evolution equation and is proportional to fourth order correlations. Using a EDQNM normalization scheme, one can identify a part of $\mathcal{G}_0$ proportional to $< \beta^*_q \beta'_s \beta''_t >$ which produces an amplitude dependent correction to the linear frequencies, $\Delta\omega$, and a part that can be expressed as the product of two quartic correlations. As with the zonal-flow-mediated nonlinear energy transfer, a turbulent correlation time for the three wave interaction can be identified and given by

$$\tau_{qst} = \frac{1}{i[\hat{\omega}''_t + \hat{\omega}'_s - \hat{\omega}^*_q]}. \tag{104}$$

In steady state, Eq. (103) has a solution of the form $< \beta^*_q \beta'_s \beta''_t > \sim \tau_{qst} C^2$, which indicates that large values of correlation times produce large nonlinear energy transfer. Using these results, the turbulent closure relations allow one to rewrite Eq. (102) the evolution equation for quadratic quantities

$$\frac{d}{dt} < \beta^*_q \beta_p >= i(\omega^*_q - \omega_p) < \beta^*_q \beta_p >$$

$$+ \sum_{k',s,t}{}' C_{pst}(k,k') \tau_{qst} \sum_{mn} [C^*_{qmn}(k,k') < \beta'_s \beta'^*_m >< \beta''_t \beta''^*_n >$$

$$+ C^*_{qmn}(k,k'') < \beta''_t \beta''^*_m >< \beta'_s \beta'^*_n >$$

$$+ C_{smn}(k',k) < \beta^*_q \beta_m >< \beta''_t \beta''^*_n >$$

$$+ C_{smn}(k',-k'') < \beta''_t \beta''^*_m >< \beta^*_q \beta_n >$$

$$+ C_{tmn}(k'',k) < \beta^*_q \beta_m >< \beta'_s \beta'^*_n >$$

$$+ C_{tmn}(k'',-k') < \beta'_s \beta'^*_m >< \beta^*_q \beta_n >]$$

$$+\sum_{k',s,t}{}' C^*_{qst}(k,k')\tau^*_{pst}[\sum_{mn} C_{pmn}(k,k') < \beta'^*_s \beta'_m >< \beta''^*_t \beta''_n >$$

$$+C_{pmn}(k,k'') < \beta''^*_t \beta''_m >< \beta'^*_s \beta'_n >$$

$$+C^*_{smn}(k',k) < \beta_p \beta^*_m >< \beta''^*_t \beta''_n >$$

$$+C^*_{smn}(k',-k'') < \beta''^*_t \beta''_m >< \beta_p \beta^*_n >$$

$$+C^*_{tmn}(k'',k) < \beta_p \beta^*_m >< \beta'^*_s \beta'_n >$$

$$+C^*_{tmn}(k'',-k') < \beta'^*_s \beta'_m >< \beta_p \beta^*_n >]. \tag{105}$$

The dominant contributions come from terms whose product of turbulent correlation time, turbulence level (which includes cross correlations) and coupling coefficients are largest. Large turbulent correlation times, by themselves, often point to the dominant transfer channels. As we shall see in the following section, for 'slab-like' ITG modes, the largest τ_{qst} corresponds to those involving an instability, a damped mode and a marginally-stable mode ($\sim \tau_{123}$ and cyclic permutations). In this case, the dominant nonlinear energy transfer is mediated by the marginal mode enabling energy transfer from the unstable to damped modes.

The steady solutions to Eq. (105) yield nine coupled algebraic equations for the quadratic quantities $< \beta_i \beta^*_j >$. While a general solution to these equations cannot be easily found, it is clear the saturated turbulence satisfies the scaling rule $< \beta_i \beta^*_j > \sim \gamma/(\tau C^2)$. For the case, where τ_{123} dominates, turbulence saturates at the level

$$< \beta_i \beta^*_j > \sim \frac{\gamma}{\tau_{123} C_{123} C}, \tag{106}$$

implying the turbulent heat flux scales inversely with the turbulent correlation time $Q \sim (\tau_{123} C_{123})^{-1}$.

C. Quantifying nonlinear transfer rates

Quantification of the two, theoretically-derived, turbulent saturation scenarios previously presented will be performed in the this section through numerical calculation. These results highlight the important role geometry plays in setting the relative strength of the non-zonal vs. zonal-flow-mediated transfer channels and the usefulness of the theory in providing a target function in stellarator design optimization schemes. Two physically relevant, neoclassical-transport-optimized stellarator configurations will be considered: the QHS HSX vacuum configuration [10] and the QAS NCSX $\beta = 4.2\%$ configuration [11]. In both nonlinear energy transfer scenarios, estimates for turbulent transport levels and corresponding turbulent heat fluxes are found to scale inversely with the turbulent correlation time weighted by the coupling coefficient, which provides the natural quantity to examine numerically for each configuration.

The numerical calculation is performed by directly solving Eq. (54) for the complex linear ITG frequencies in the absence of dissipation, $\hat{\mu} = \hat{D} = \hat{\chi} = 0$. The important geometric information enters through the eigenmode averaged quantities, $< D_k >_0$, $< B_k >_0$ and $< k^2_\parallel >_0$. To avoid the step of solving Eq. (50) numerically for the eigenvalue and eigenfunction, an eigenmode ansatz is made using insights gleaned from linear gyrokinetic simulation. In the strongly driven limit considered here, $a/L_T = \epsilon_T = 3$, $a/L_n = 0$, linear eigenmodes at (k_x, k_y) computed by the GENE code [47] are observed to have approximately Gaussian shape and are localized along the field line to a region close to the ballooning angle $\eta_k = k_x/k_y(d\iota/d\rho)^{-1}$ where the stabilizing effects of $k^2_\perp \rho^2_s$ effects are minimized and adjacent local shear spikes are large enough to provide confinement; see Appendix A for further discussion. This allows us to implement a procedure where for a given η_k, the correct mode width and location can be found for the analytic model and the quantities $< D_k >_0$, $< B_k >_0$ and $< k^2_\parallel >_0$ can be evaluated.

In figures (1) and (2), contour plots of the linear growth rate spectrum from the analytic model for QAS and QHS, respectively, are provided as a function of k_x and k_y. The equivalent growth contour plots are provided in figures (3) and (4) for the two configurations using GENE to provide gyrokinetic predictions While there are some quantitative differences, the figures indicate that the analytic model [Eq. (54)] emulates many of the linear stability features predicted in gyrokinetic calculations. Linear growth rates are higher in QHS relative to QAS at nearly all values of k_x and k_y. Qualitatively similar growth rate spectra are observed between the analytic model and gyrokinetic

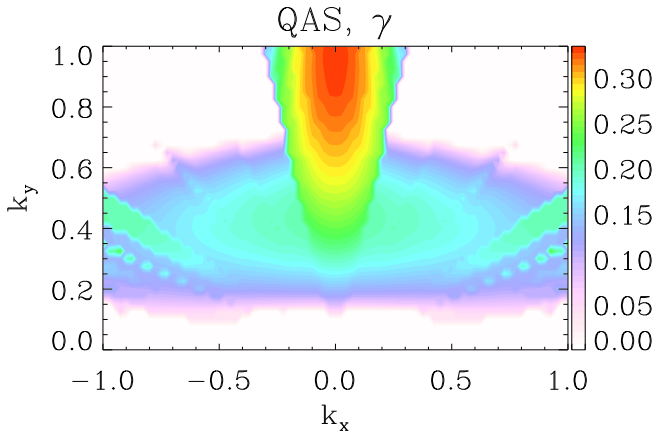

FIG. 1. Contours of the peak linear growth rates for the NCSX configuration as predicted by Eq. (54) as a function of k_x and k_y.

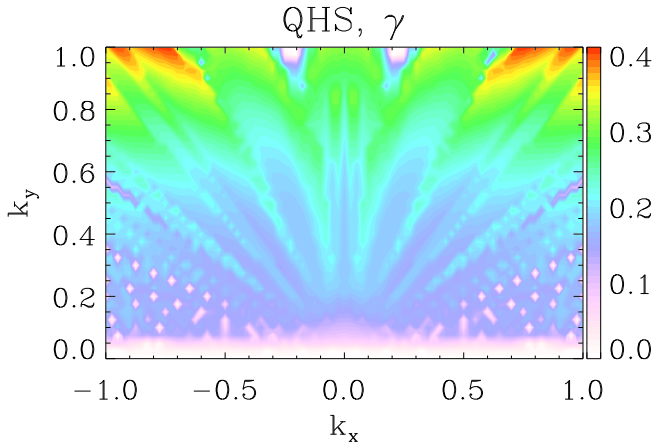

FIG. 2. Contours of the peak linear growth rates for the HSX configuration as predicted by Eq. (54) as a function of k_x and k_y.

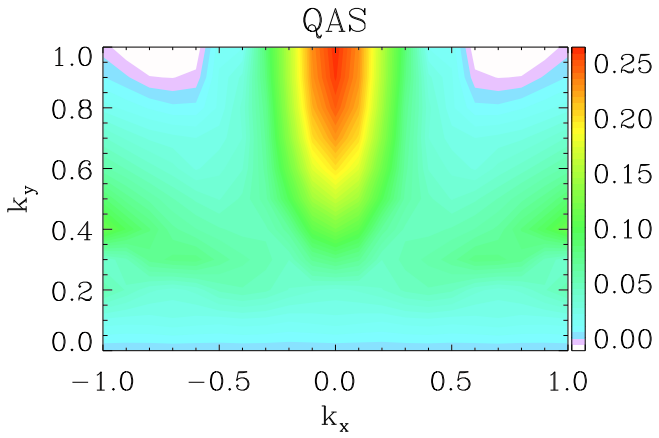

FIG. 3. Contours of the peak linear growth rates for the NCSX configuration as predicted by gyrokinetic calculations using GENE as a function of k_x and k_y.

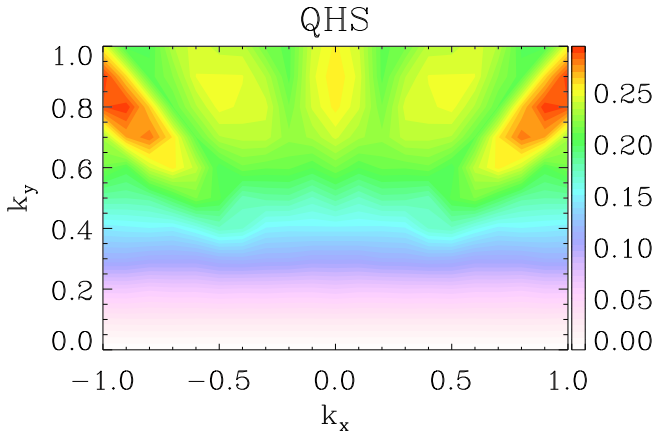

FIG. 4. Contours of the peak linear growth rates for the HSX configuration as predicted by gyrokinetic calculations using GENE as a function of k_x and k_y.

calculation, and most importantly, the finite-k_x dependence of both QAS and QHS are recovered by the fluid model. The QHS growth rate spectrum exhibits 'ridges' and 'valleys', which occur when a mode localized to a particular drift well and stabilized with increasing k_x due to FLR effects, jumps to a different drift well where $k_\perp^2$ effects are smaller, increasing growth rates. This effect is more pronounced in QHS than QAS, as $d\iota/d\rho$ for HSX is smaller by an order of magnitude compared to NCSX and provides only a weak confining effect, allowing the mode to strongly balloon far from $k_x = 0$.

Evaluation of the turbulent correlation lifetime, τ_{qst}, is done using only the complex linear frequencies, as nonlinear gyrokinetic simulation of collisionless ITG turbulence for both QAS and QHS at $\epsilon_T = 3$ indicate nonlinear modifications to the linear frequencies are small at low-k. As both configurations under consideration are neoclassically optimized, in practice the collisionless zonal flow frequency is quite small compared to the eigenmode frequencies. Nonlinear gyrokinetic simulations indicate $\omega_F \ll 10^{-6}$ for both configurations. As such, we use the approximation $\omega_F = 0$ in the following. The matrix elements and coupling coefficients are then calculated with only the linear frequencies. Finite Larmor radius effects in Eqs. (69)–(74) given by $\{B_{k'k}\}$ and $\{B_{k'-kk}\}$ are found to be negligible and dropped in the following evaluations.

As energy transfers involving zonal modes represents a special coupling, the nonlinear energy transfer to stable modes at wavenumber $\mathbf{k}$ is shown for zonal-flow-mediated energy transfer independently from non-zonal energy transfer. In the case of zonal-flow-mediated energy transfer, nonlinear energy transfer is governed by Eq. (88) with the quantity $\tau_{pqF}C_{pqF}$ emerging as an important metric for quantifying the rate of nonlinear energy transfer involving eigenmodes p and q. The quantity τ_{pqF} denotes a turbulent correlation as defined in Eq. (87) as a three wave mismatch frequency and C_{pqF} given in Eq. (69) denotes a geometric coupling coefficient. In practice the largest of nonlinear energy transfer rates correspond to those involving an unstable mode and a damped mode (quantified by $\tau_{12F}C_{12F}$). From Eq. (54), note that τ_{12F} becomes large in the limit of weak k_x dependence of the growth rate and small zonal flow damping frequency.

Figures (5) and (6) provide quantitative estimates for QAS and QHS, respectively, of zonal-flow-catalyzed transfer as measured by the quantity $\tau_{12F}C_{12F}$. In both figures, contours of $|\tau_{12F}C_{12F}|$ are plotted as a function of the k_y used to evaluate the unstable mode (ω_1) at $k_x = 0$ and the k_x of the zonal field, with the damped eigenfrequency evaluated at the corresponding k_x, k_y pair in accordance to the rule $\mathbf{k}'' = \mathbf{k} - \mathbf{k}'$. The peak regions of $|\tau_{12F}C_{12F}|$ for QAS in Figure (5) are located close to $k_x = 0$, due to strong k_x dependence of the toroidal ITG modes in QAS and similar to an axisymmetric configuration. The regions of large $|\tau_{12F}C_{12F}|$ for QHS can occur at large k_x and due to the slab-like nature of ITG modes in HSX, tend to lie in the growth rate 'valleys', where the finite-k_x mode frequencies match more closely the $k_x = 0$ mode frequency. In both configurations, nonlinear gyrokinetic simulation indicates the energy containing scales are confined to $|k_x| \leq 0.2$ and $k_y \leq 1$ and is denoted by the dashed vertical lines in Figures (5) and (6). Since the total energy transfer is proportional to the energy in the unstable mode and zonal flow, our figure of merit is the average over the energy containing wavenumbers of $|\tau_{12F}C_{12F}|$ defined by

$$\langle|\tau_{12F}C_{12F}|\rangle = \frac{\sum_{k_x=0}^{k_x=0.2}\sum_{k_y=0}^{k_y=1}|\tau_{12F}C_{12F}|}{\sum_{k_x=0}^{k_x=0.2}\sum_{k_y=0}^{k_y=1}}, \tag{107}$$

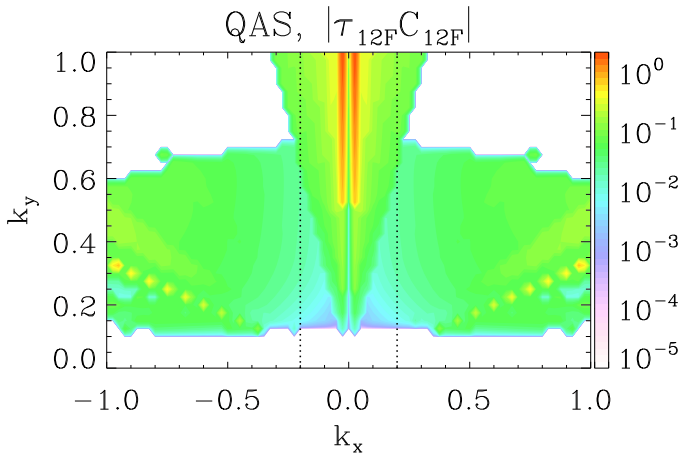

FIG. 5. Contours of the quantity $|\tau_{12F}C_{12F}|$ for the NCSX configuration is plotted as a function of k_x and k_y.

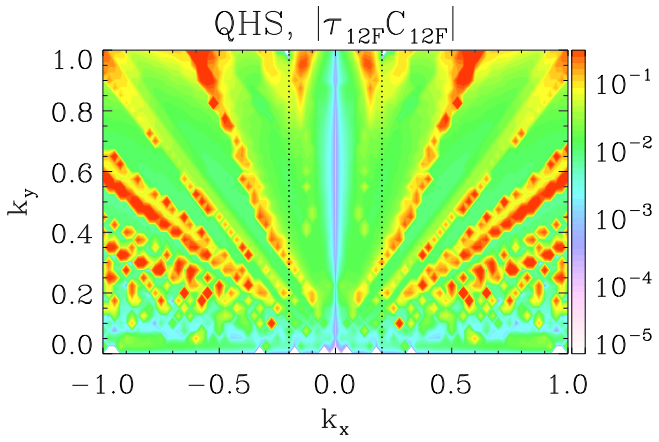

FIG. 6. Contours of the quantity $|\tau_{12F}C_{12F}|$ for the HSX configuration is plotted as a function of k_x and k_y.

We find that $\langle|\tau_{12F}C_{12F}|\rangle$ for QAS is roughly ten times larger than for QHS, indicating the zonal flows play a more dominant role in transferring energy in QAS and is summarized in Table I.

In Figures (7) and (8), contours of the peak value of the non-zonal energy transfer quantity $|\tau_{qst}C_{qst}|$ are plotted as a function of k_x and k_y for QAS and QHS. For these figures, at each k_x, k_y location all combinations of the three linear eigenfrequencies are surveyed for different choices of the labels q, s and t and the largest value used in the plot. Additionally, the peak choice is obtained by scanning over all values of k'. Again, there are detailed differences between the properties of the non-zonal energy transfer for the two different configurations as a function of wavenumber, however, the important property to note is the scale in the plots. Typical peak values of non-zonal energy transfer is considerably larger for QHS than QAS and averaging over the energy containing scales as before indicates the non-zonal energy transfer channel is correspondingly stronger for QHS than QAS,

$$\frac{\left\langle|\tau_{1st}C_{1st}|^{QHS}\right\rangle}{\left\langle|\tau_{1st}C_{1st}|^{QAS}\right\rangle} \sim 10^2, \tag{108}$$

and is also given in Table I. This suggests that non-zonal energy transfer plays a much larger role in QHS configurations than in QAS configurations. One should note that for QAS, $|\tau_{12F}C_{12F}|$ and $|\tau_{1st}C_{1st}|$ are of comparable order. However, as shown in Eq. (88), the nonlinear energy transfer rate involving zonal flows scales with zonal flow energy density ($\sim \tau_{12F}C_{12F}|\Phi^Z|^2$), whereas as the corresponding expression for non-zonal energy transfer [Eq. (105)] scales with turbulence energy density ($\sim \tau_{qst}C_{qst}|\beta|^2$). As the zonal amplitudes in nonlinear gyrokinetic simulations are considerably larger than non-zonal amplitudes this suggests the energy transfer to stable modes in QAS is dominated by the zonal-flow-catalyzed energy transfer, similar to tokamak observations.

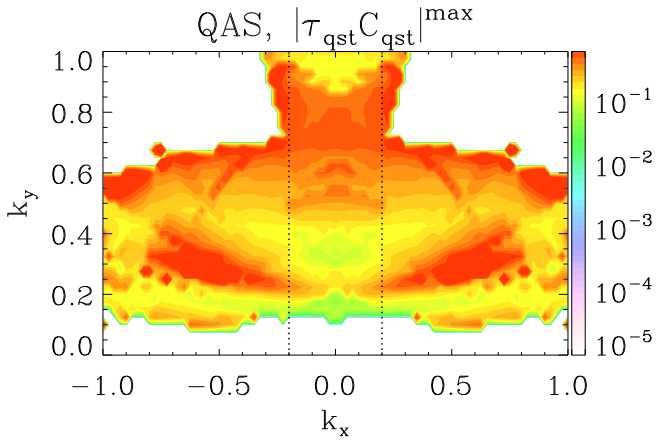

FIG. 7. Contours of the quantity $|\tau_{qst}C_{qst}|$ for the NCSX configuration is plotted as a function of k_x and k_y using the largest values from all possible choices for q, s and t.

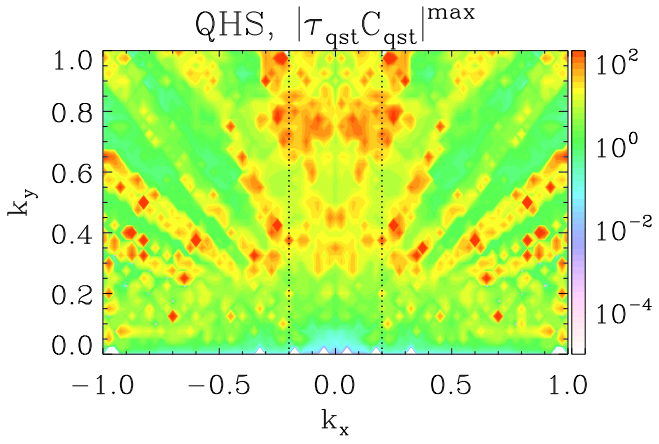

FIG. 8. Contours of the quantity $|\tau_{qst}C_{qst}|$ for the HSX configuration is plotted as a function of k_x and k_y using the largest values from all possible choices for q, s and t.

The difference between QAS and QHS in non-zonal energy transfer is primarily due to differences in magnetic geometry. In QHS stellarators, ITG modes are more slab-like due to the relatively short connection length. While short connection lengths are known to have adverse effects on QHS with respect to linear instability, this work indicates importantly that this shortcoming in QHS may be overcome by having more vigorous nonlinear saturation physics facilitated by robust non-zonal energy transfer. This result is in sharp contrast to the properties of tokamaks and the QAS configuration where the zonal flow is known to play the dominant role in ITG turbulence saturation. Indeed, there are indications from nonlinear GENE simulations that zonal flows play little role in ITG turbulent saturation in HSX geometry [48].

It is instructive to examine which combination of q, s and t maximize $|\tau_{qst}C_{qst}|$ for a given $\mathbf{k}$ and is shown in Figures

Configuration	$\langle\|\tau_{12F}C_{12F}\|\rangle$	$\langle\|\tau_{qst}C_{qst}\|\rangle$
QAS	0.159	0.261
QHS	0.027	23.89

TABLE I. Zonal-flow-catalyzed ($|\tau_{12F}C_{12F}|$) and non-zonal energy transfer ($|\tau_{qst}C_{qst}|$) averaged over the energy containing scales $|k_x| \leq 0.2$, $k_y \leq 1$ for the QAS and QHS configurations.

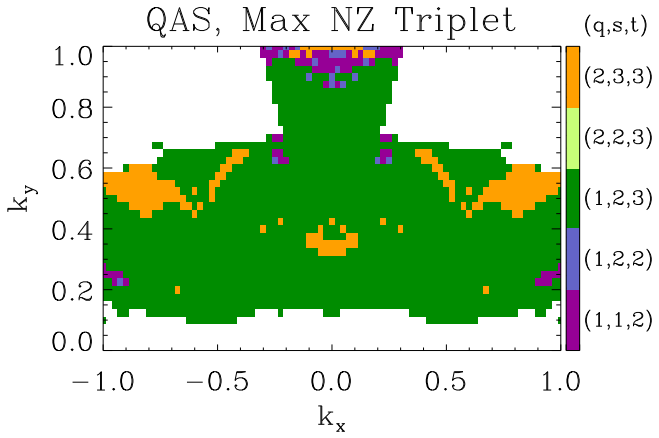

FIG. 9. The largest choice for p, q and r for the quantity $|\tau_{qst}C_{qst}|$ for NCSX geometry is plotted as a function of k_x and k_y. The region colored green denotes the dominance of three interactions that involve an unstable mode, a damped mode and a marginally stable mode.

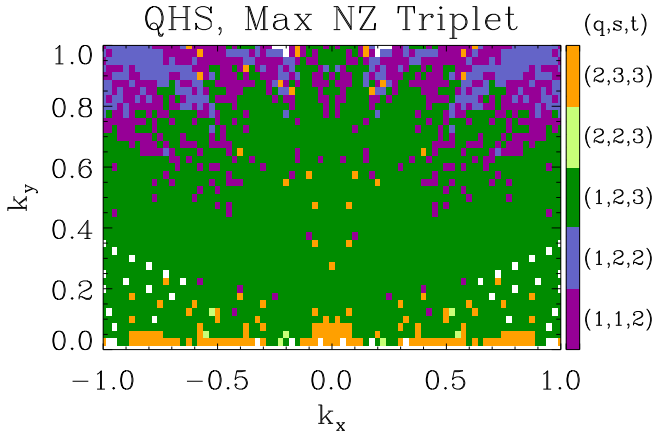

FIG. 10. The largest choice for p, q and r for the quantity $|\tau_{qst}C_{qst}|$ for HSX geometry is plotted as a function of k_x and k_y.The region colored green denotes the dominance of three interactions that involve an unstable mode, a damped mode and a marginally stable mode.

(9) and (10). For both QAS and QHS, we find that the largest nonlinear energy transfer rates for non-zonal energy transfer involve coupling of an unstable mode, a damped mode and a marginally stable mode as measured by $\tau_{123}C_{123}$ (and cyclic permutations). This provides an important, configuration independent, information and suggests that a route to reducing ITG turbulent transport in 3D configurations is to maximize the target functions $|\tau_{12F}C_{12F}|$ and $|\tau_{123}C_{123}|$ in stellarator design optimization schemes.

VI. SUMMARY AND DISCUSSION

A three-field fluid model is developed to describe ion temperature gradient turbulent saturation processes in stellarators. The model uses a ballooning formalism and accommodates general three-dimensional equilibrium geometry. The theory relies on the premise that turbulent saturation is controlled by nonlinear energy transfer from unstable to stable eigenmodes. In the formulation presented here, this energy transfer is enabled by a third mode whose precise identity depends upon the magnetic geometry. The theory is developed to accommodate two scenarios, one where the zonal flow is the dominant catalyst for nonlinear energy transfer and one where an additional turbulent eigenmode provides the dominant nonlinear energy transfer channel. The nonlinear energy transfer physics is quantified by the

product of a turbulent correlation lifetime and a geometric coupling coefficient. The turbulent correlation lifetime is determined by a three-wave frequency mismatch, which at long wavelength can be calculated from the sum of linear eigenfrequencies.

Proxies for turbulent saturation optimization are identified. The two nonlinear saturation scenarios are quantified by the quantities $\tau_{12F}C_{12F}$ and $\tau_{123}C_{123}$, with large values of these entities denoting large nonlinear energy transfer rates and correspondingly low values of turbulent fluctuations and turbulent transport. The turbulent correlation time τ_{12F} [as given in Eq. (87)] denotes a three wave interaction where the zonal flow plays the role of a catalyst for transferring energy from unstable to damped modes. Non-zonal energy transfer is catalyzed by a marginally stable eigenmode and quantified by the turbulent correlation time τ_{123} as described by Eq. (104). In both turbulent saturation scenarios, turbulent transport coefficients scale inversely with the product of the turbulent correlation time and its associated coupling coefficient of the dominant nonlinear energy transfer process.

Quantification of these metrics are provided for two classes of quasi-symmetric stellarators configurations. These calculations suggest that quasi-helically symmetric configurations have multiple scenarios for achieving turbulent saturation. Both zonal-flow-catalyzed nonlinear energy transfer and energy transfer enabled by marginal modes can play a role for QHS, while the nonlinear energy transfer present in QAS stellarators is dominated by zonal-flow-catalyzed transfer. This suggests that QHS configurations may have an intrinsic advantage with regard to turbulent saturation processes that can offset their apparent disadvantages with respect to linear instability. More importantly, by identifying a definitive route to turbulent saturation, efforts to accentuate the strength of the dominate nonlinear energy transfer channel can be exploited in stellarator optimization schemes to reduce turbulent transport.

Large values of $\tau_{12F}C_{12F}$ and $\tau_{123}C_{123}$ lead to large values of nonlinear energy transfer and therefore assist in lowering transport levels. To estimate the impact of τC on transport coefficients, steady state solutions to the nonlinear evolution equations for the turbulent energy densities can found and used in Eq. (79) to calculate the turbulent heat flux. The theory presented here suggests that turbulent saturation processes provide a correction to mixing length estimates for turbulent ion heat conductivity, $\chi \sim g\gamma/k_\perp^2$ where the scale factor g scales inversely with τC for the dominant nonlinear saturation mechanism. This implies that minimizing $\gamma/(\tau_{12F}C_{12F})$ and/or $\gamma/(\tau_{123}C_{123})$ is a route to reducing ITG-induced turbulent transport in stellarator optimization procedures.

The initial turbulent saturation studies for stellarators pursued here emphasized ion temperature gradient driven turbulence. However, one might also envision addressing the saturation properties of trapped electron mode (TEM) turbulence in stellarators as well. Unlike quasi-isodynamic configurations [49], quasi-symmetric stellarators are anticipated to have poor TEM properties, as trapped particle populations reside in regions with unfavorable field line curvature. However, it might be possible to overcome the unfavorable linear stability properties by appealing to a strong nonlinear saturation mechanism. Indeed, nonlinear gyrokinetic simulations of trapped electron turbulence in HSX geometry exhibit significant signatures of damped eigenmodes as a prominent feature of saturated turbulence [50].

An important next step in this work is to implement the turbulent optimization metrics developed here in stellarator optimization design studies. This work suggests reduced ITG turbulent transport can be realized by maximizing the the quantities $\tau_{12F}C_{12F}$ and $\tau_{123}C_{123}$ to accentuate large nonlinear energy transfer. If such configurations can be found, it would be of great interest to test the predictions of the theory presented here against nonlinear gyrokinetic simulations and ultimately a new class of turbulence-optimized stellarator experiments.

ACKNOWLEDGMENTS

This work was supported by the U. S. Department of Energy under Grant no. DE-FG02-99ER54546, DE-FG02-89ER53291 and DE-FG02-93ER54222.

Appendix A: ITG linear stability

Linear instability of non-zonal fields from our model is governed by an ordinary differential equation of the form

$$(\mathbf{B}\cdot\nabla)[\frac{L_{eq}^2}{B^2}(\mathbf{B}\cdot\nabla\Phi)] + V\Phi = 0, \tag{A1}$$

where

$$V = \frac{\omega^3}{k_y\epsilon_T + \omega} + \omega^2 B_k + \omega D_k. \tag{A2}$$

The general solution requires a numerical treatment for complex 3D fields. However, we can come up with approximate expressions using insight from past numerical treatments and observations of the properties of magnetic geometry in stellarators. Crudely, there are two classes of solutions, one set of eigenmodes that are localized within one helical bump in the bad curvature region and another set of eigenmodes that are extended along the field line.

For the first class of modes, we note that the localization is primarily due to the properties of the local magnetic shear. Generally, in stellarator configurations the local shear along the field line has two regions, a region of small local 'tokamak-like' magnetic shear and localized regions with large 'stellarator-like' magnetic shear. The average of these two regions yields the average magnetic shear which very often happens to be rather small (as in W7X and HSX for example). The localized jumps in magnetic shear tend to occur in the corner regions where the magnetic field line torsion abruptly changes. As such, the integrated local shear (Λ) experiences jumps at the these locations. As both D_k and B_k contain terms that scale with Λ, the quantity V jumps up as the field line goes through the large local shear region. To crudely model this feature (for illustrative purposes), we can model the quantity $V(\eta)$ as

$$\begin{aligned} &= V_1 \qquad \eta < -\eta_0 \\ V(\eta) &= V_0 \qquad -\eta_0 < \eta < \eta_0 \\ &= V_1 \qquad \eta_0 < \eta, \end{aligned} \tag{A3}$$

where $V_1 > V_0$, the eigenmode equation satisfies $d^2\Phi/d\eta^2 + V(\eta)\Phi = 0$ and the field line label η is defined by

$$\eta = \int_0^\eta d\eta' \frac{B^2}{\mathbf{B}\cdot\nabla\eta'} \Big(\oint_0^{2\pi} \frac{d\eta'}{2\pi} \frac{B^2}{\mathbf{B}\cdot\nabla\eta'} \Big)^{-1}, \tag{A4}$$

with the first jump in local shear occurring at $\eta = \pm\eta_0$. Subsequent jumps in the local shear occur but we will be mostly interested in eigenmodes bound within the dominant well structure associated with the first jump. The eigenmode equation is now reduced to a classic quantum mechanical potential well problem. Bounded eigenmodes can be constructed if $V_0 < 0$ and $V_1 > 0$. In this case, eigenmodes have the shape $\phi \sim \cos(\eta\sqrt{-V_0}), \sin(\eta\sqrt{-V_0})$ for $|\eta| < \eta_0$ and $\phi \sim e^{-|\eta|\sqrt{V_1}}$ for $|\eta| > \eta_0$. Eigenvalues for the even parity modes satisfy

$$\tan(\eta_0\sqrt{-V_0}) = \sqrt{\frac{V_1}{-V_0}}, \tag{A5}$$

which in the limit of a large jump in the local shear at $\eta = \eta_0$ yields the eigenvalue condition $\cos(\eta_0\sqrt{-V_0}) = 0$ for the even parity modes which corresponds to

$$\frac{\pi^2}{4\eta_0^2}(1+2k)^2 + V_0 = 0, \tag{A6}$$

for integer values of k. This is essentially the "boxed" ITG mode of [44]. In this form, it's clear that the effect of the local shear jumps is to force $k_{||}$ to take a particular value set by the geometry. For QHS devices, we'd expect the parallel wave number to scale with the effective transform $k_{||} \sim (N - \iota)/R_o$. For this class of modes, effectively one can treat $k_{||}$ as a parameter set by the magnetic geometry and the treatment of Section III is appropriate.

Linear eigenmodes can also be found that have an extended length along the field line. In the special case of weak averaged shear ($d\iota/d\rho \to 0$), Eq. (A1) takes the form of a generalized Mathieu-like equation [51] with localization due to the 3D nature of the local shear [52, 53].

Instabilities for long wavelength modes that depend explicitly on a weak but non-zero averaged magnetic shear can also be uncovered using a two-scale analysis. For this case, a short scale η' or order the connection length and a long scale $z = \eta s_0$ that depends upon the averaged magnetic shear $s_0 = \psi'(d\iota/d\rho)B_0^{-1}$ is identified. Following standard techniques one derive an equation for the envelope of the eigenmode in the variable z that yields bounded eigenfunctions and physical eigenvalues that are either are real or complex conjugate pairs that are nearly independent of k_x.

Appendix B: Linear eigenmode expansion

The governing equations for non-zonal modes can be expressed in terms of an expansion of the linear eigenmodes β_1, β_2 and β_3 at each $\mathbf{k}$. These quantities are related to the basic fluid quantities by a matrix M_k through the relation $\vec{\Phi}_k = M_k\vec{\beta}$ where $\vec{\Phi}_k = (\Phi_k, T_k, G_k)^T$ and

$$M_k = \begin{pmatrix} 1 & 1 & 1 \\ \frac{k_y\epsilon_T}{\omega_1} & \frac{k_y\epsilon_T}{\omega_2} & \frac{k_y\epsilon_T}{\omega_3} \\ (\frac{i}{\omega_1} + \frac{ik_y\epsilon_T}{\omega_1^2}) & (\frac{i}{\omega_2} + \frac{ik_y\epsilon_T}{\omega_2^2}) & (\frac{i}{\omega_3} + \frac{ik_y\epsilon_T}{\omega_3^2}) \end{pmatrix}. \tag{B1}$$

The inverse of this matrix is given by

$$M_k^{-1} = M_0 \begin{pmatrix} \frac{k_2^2\epsilon_T^2}{\omega_2^2\omega_3^2}(\omega_2-\omega_3) & \frac{1}{\omega_2}+\frac{k_y\epsilon_T}{\omega_2^2}-\frac{1}{\omega_3}+\frac{k_2\epsilon_T}{\omega_3^2} & i\frac{k_y\epsilon_T}{\omega_2\omega_3}(\omega_3-\omega_2) \\ \frac{k_y^2\epsilon_T^2}{\omega_3^2\omega_1^2}(\omega_3-\omega_1) & \frac{1}{\omega_3}+\frac{k_y\epsilon_T}{\omega_3^2}-\frac{1}{\omega_1}+\frac{k_y\epsilon_T}{\omega_1^2} & i\frac{k_2\epsilon_T}{\omega_3\omega_1}(\omega_1-\omega_3) \\ \frac{k_y^2\epsilon_T^2}{\omega_1^2\omega_2^2}(\omega_1-\omega_2) & \frac{1}{\omega_1}+\frac{k_y\epsilon_T}{\omega_1^2}-\frac{1}{\omega_2}+\frac{k_y\epsilon_T}{\omega_2^2} & i\frac{k_2\epsilon_T}{\omega_1\omega_2}(\omega_2-\omega_1), \end{pmatrix} \tag{B2}$$

where $M_0 = -i\lambda^2/(k_y^2\epsilon_T^2\sqrt{4A^3+27C^2})$.

Appendix C: Nonlinear frequency shifts

The quantities from Eq. (84) labeled $\Delta\omega$ denote corrections to the complex frequencies that are quadratic in turbulence field amplitudes. In the limit the zonal flow induced nonlinear transfer dominates, nonlinear frequency shifts can be calculated by iterating on the evolution equations. In this case, the zonal flow obeys Eq. (75) and the non-zonal modes evolve according to Eq. (81). Using these evolution equations and standard renormalization techniques, an expression for the nonlinear frequency shift for the zonal flows can be derived. This is given by

$$\Delta\omega_F = -\sum_{k'qrs} \frac{C_{Fqr}(k,k')\hat{C}^Z_{qrs}}{\omega'_q+\Delta\omega'_q+\omega''_r+\Delta\omega''_r}, \tag{C1}$$

where

$$\hat{C}^Z_{qrs} = C_{qsF}(k',-k'') < \beta''_r\beta''^*_s > \\ +C_{rsF}(k'',-k') < \beta'_q\beta'^*_s > \tag{C2}$$

A similar procedure allows one to derive the nonlinear frequency shifts for the modes [54]

$$\Delta\omega_p = -\sum_q \frac{C_{pqF}(k,k')C_{qpF}(k',k)|\Phi^Z_{k-k'}|^2}{\omega'_q+\Delta\omega'_q+\omega''_F+\Delta\omega''_F}. \tag{C3}$$

The latter condition yields the scaling $\Delta\omega \sim C^2|\Phi^Z|^2/\omega$ in the weak turbulence limit and $\Delta\omega \sim C|\Phi^Z|$ in the strong turbulence limit. The corresponding condition for the first equation yields $\Delta\omega_F \sim C^2|\beta|^2/\omega$ in the weak turbulence limit and $\Delta\omega_F \sim C^2|\beta|^2/\Delta\omega \sim C|\beta|^2/|\Phi^Z|$ in the strong turbulence limit. These estimates are made assuming zonal flows dominate the nonlinear physics with $|\Phi^Z|^2 >> |\beta|^2$.

For the case where nonlinear energy transfer is dominated by non-zonal modes, the evolution equations for the mode is approximately given by Eq. (102). In this case, the zonal fields play a sub-dominant role. The nonlinear frequency shift in this case are given by

$$\Delta\omega_p = -\sum_{k'qrs} \frac{C_{pqr}(k,k')\hat{C}_{pqr}}{\omega'_q+\Delta\omega'_q+\omega''_r+\Delta\omega''_r}, \tag{C4}$$

where

$$\hat{C}_{pqr} = [C_{qps}(k',k)+C_{qsp}(k',-k'')] < \beta''_r\beta''^*_s > \\ +[C_{rps}(k'',k)+C_{rsp}(k'',-k')] < \beta'_q\beta'^*_s > . \tag{C5}$$

In the weak turbulence limit this relation yields the scaling $\Delta\omega \sim C^2|\beta|^2/\omega$. In the strong turbulence limit, we find the scaling $\Delta\omega \sim C|\beta|$.

[1] D. R. Hatch, P. W. Terry, F. Jenko, F. Merz and W. M. Nevins, *Phys. Rev. Lett.* **106**, 115003 (2011).
[2] K. Makwana, P. W. Terry, and J.-H. Kim, *Phys. Plasmas* **19**, 062310 (2012).
[3] K. Makwana, P. W. Terry, M. J. Pueschel and D. R. Hatch, *Phys. Rev. Lett.* **112**, 095002 (2014).

[4] D. A. Spong, S. P. Hirshman, L. A. Berry, J. F. Lyon, R. H. Fowler, D. J. Stricker, M. J. Cole, B. N. Nelson, D. E. Williamson, A. S. Ware, D. Alban, R. Sanchez, G. Y. Fu, D. A. Monticello, W. H. Miner, and P. M. Valanju , *Nucl. Fusion* **41**, 711 (2001).
[5] H. E. Mynick, T. K. Chu and A. H. Boozer, *Phys. Rev. Lett.* **48**, 322 (1982)
[6] J. Nuhrenberg, W. Lotz, P. Merkel, C. Nuhrenberg, U. Schwenn and E. Strumberger, *Fusion Technology* **27**, 71 Supplement S (1995).
[7] A. H. Boozer, *Phys. Fluids* **26**, 496 (1983).
[8] H. Nuhrenberg and R. Zille, *Phys. Lett. A* **129**, 113 (1988).
[9] C. Beidler, G. Grieger, F. Herrnegger, E. Harmeyer, J. Kisslinger, W. Lotz, H. Maassbeerg, P. Merkel, J. Nuhrenberg, F. Rau, J. Sapper, F. Sardei, R. Scardovelli, A. Schluter and A. Wobig, *Fusion Technol.* **17**, 148 (1990).
[10] J. N. Talmadge, V. Sakaguchi, F. S. B. Anderson, D. T. Anderson and A. F. Almagri, *Phys. Plasmas* **8**, 5165 (2001).
[11] G. H. Neilson, M. C. Zarnstorff, J. F. Lyon and the NCSX Team, *J. Plasma Fusion Res.* **78**, 214 (2002).
[12] D. A. Spong, S. P. Hirshman, J. C. Whitson, D. B. Batchelor, R. Sanchez, B. A. Carreras, V. E. Lynch, J. F. Lyon, P, M. Valanju, W. H. Miner, P. E. Moroz, M. C. Zarnstroff, D. A. Monticello, A. S. Ware and L. Garcia, *Nuclear Fusion* **40**, 563 (2000).
[13] H. E. Mynick, N. Pomphrey, P. Xanthopoulos, *Phys. Rev. Lett.* **105**, 095004 (2010).
[14] H. E. Mynick, N. Pomphrey, and P. Xanthopoulos, *Phys. Plasmas* **18**, 056101 (2011).
[15] H. Mynick, P. Xanthopoulos, B. Faber, M. Lucia, M. Rorvig and J. N. Talmadge, *Plasma Phys. Control. Fusion* **56**, 094001 (2014).
[16] J. H. E. Proll, H.E. Mynick, P. Xanthopoulos, S. A. Lazerson, and B. J. Faber, *Plasma Phys. Control. Fusion* **58**, 014006 (2016).
[17] M. J. Pueschel, B. J. Faber, J. Citrin, C. C. Hegna, P. W. Terry and D. R. Hatch, *Phys. Rev. Lett.* **116**, 085001 (2016).
[18] J. M. Canik, D. T. Anderson, F. S. B. Anderson, K. M. Likin, J. N. Talmadge and K. Zhai, *Phys. Rev. Lett.* **98**, 085002 (2007).
[19] G. M. Weir, B. J. Faber, K. M. Likin, J. N. Talmadge, D. T. Anderson and F. S. B. Anderson, *Phys. Plasmas* **22**, 056107 (2015).
[20] T. Rafiq and C. C. Hegna, *Phys. Plasmas* **13**, 062501 (2006).
[21] W. Guttenfelder, J. Lore, D. T. Anderson, F. S. B. Anderon, J. M. Canik, W. Dorland, K. M. Likin and J. N. Talmadge, *Phys. Rev. Lett.* **101**, 215002 (2008).
[22] B. J. Faber, M. J. Puschel, J. H. E. Proll, P. Xanthopoulos, P. W. Terry, C. C. Hegna, G. M. Weir, K. M. Likin and J. N. Talmadge, *Phys. Plasmas* **22**, 072305 (2015).
[23] G. Rewoldt, L. Ku and W. M. Tang, *Phys. Plasmas* **12**, 102512 (2005).
[24] C. C. Hegna and S. R. Hudson, *Phys. Rev. Lett.* **87**, 035001 (2001).
[25] P. Helander, T. Bird, F. Jenko, R. Kleiber, G. G. Plunk, J. H. E. Proll, J. Riemann and P. Xanthopoulos *Nucl. Fusion* **55**, 053030 (2015).
[26] H. Yamada, J. H. Harris, A. Dinklage, E. Ascasibar, F. Sano, S. Okamura, J. Talmadge, U. Stroth, A. Jus, S. Murakami, M. Yokoyama, C. D. Beidler, V. Tribaldos, K. Y. Watanabe and Y. Suzuki, *Nuclear Fusion* **45** 1684 (2005).
[27] P. H. Diamond, S.-I. Itoh, K. Itoh and T. S. Hahm, *Plasma Phys. Control. Fusion* **47**, R35 (2005)
[28] M. Barnes, F. I. Parra and A. A. Schekochihin, *Phys. Rev. Lett.* **107**, 115003 (2011).
[29] G. G. Plunk, A. Banon Navarro and F. Jenko, *Plasma Phys. Control. Fusion* **57**, 045005 (2015).
[30] H. Sugama and T.-H. Watanabe, *Phys. Plasmas* **13** 012501 (2006); *Phys. Plasmas* **16**, 056101 (2007).
[31] H. E. Mynick and A. H. Boozer, *Phys. Plasmas* **14**, 072507 (2007).
[32] T.-H. Watanabe, H. Sugama and S. Ferrando-Margalet, *Phys. Rev. Lett.* **100**, 195002 (2008).
[33] P. Helander, A. Mishcenko, R. Kleiber and P. Xanthopoulos, *Plasma Phys. Control. Fusion* **53**, 054006 (2011).
[34] P. Xanthopoulos, A. Mischenko, P. Helander, H. Sugama and T.-H. Watanabe, *Phys. Rev. Lett.* **107**, 245002 (2011).
[35] K. C. Shaing, *Phys. Plasmas* **12**, 082508 (2005).
[36] M. Nunami, T.-H. Watanabe and H. Sugama, *Plasma and Fusion Research: Rapid Communications* **8**, 1203019 (2013).
[37] Z. Lin, T. S. Hahm, W. W. Lee, W. M. Tang and P. H. Diamond, *Phys. Rev. Lett.* **83**, 3645 (1999).
[38] W. Horton, B. G. Hong and W. M. Tang, *Phys. Fluids* **24**, 1077 (1981).
[39] C. Holland, P. H. Diamond, S. Champeaux, E. Kim, O. Gurcan, M. N. Rosenbluth, G. R. Tynan, N. Crocker, W. Nevins and J. Candy, *Nucl. Fusion* **43**, 761 (2003).
[40] C. C. Hegna, *Phys. Plasmas* **7**, 3921 (2000).
[41] R. L. Dewar and A. H. Glasser, *Phys. Fluids* **26**, 3038 (1983).
[42] J. Anderson, T. Rafiq, M. Nadeem and M. Persson, *Phys. Plasmas* **9**, 1629 (2002).
[43] F. L. Hinton and M. N. Rosenbluth, *Plasma Phys. Control. Fusion* **41** A653 (1999)
[44] G. G. Plunk, P. Helander, P. Xanthopoulos and J. W. Connor, *Phys. Plasmas* **21**, 032112 (2014).
[45] P. W. Terry, B. J. Faber, C. C. Hegna, V. V. Mirnov, M. J. Pueschel and G. G. Whelan, *Phys. Plasma* **25** 012308 (2018).
[46] P. W. Terry, *Phys. Rev. Lett.* **93**, 235003 (2004).
[47] F. Jenko, W. Dorland, M. Kotschenreuther and B. N. Rogers, *Phys. Plasmas* **7**, 1904 (2000).
[48] G. G. Plunk, P. Xanthopoulos and P. Helander, *Phys. Rev. Lett.* **118**, 105002 (2017).
[49] J. H. E.. Proll, P. Helander, J. W. Connor and G. G. Plunk, *Phys. Rev. Lett.* **108**, 245002 (2012).
[50] B. J. Faber, M. J. Pueschel, P. W. Terry and C. C. Hegna, *Bull. Am. Phys. Soc.* **62**, G04.00001 (2017).
[51] A. Bhattacharjee, J. E. Sedlak, P. L. Similon and M. N. Rosenbluth, *Phys. Plasms* **26**, 880 (1983).
[52] P. Cuthbert and R. L. Dewar, *Phys. Plasmas* **7**, 2302 (2000).

[53] C. C. Hegna and S. R. Hudson, *Phys. Plasmas* **9**, 2014 (2002).
[54] D. A. Baver, P. W. Terry and R. Gatto, *Phys. Plasmas* **9**, 3318 (2002).